MICROWAVE REMOTE SENSING RESPONSE OF SNOW COVERED TERRAINS

A Thesis Submitted
In Partial fulfilment of the Requirements
for the Degree of

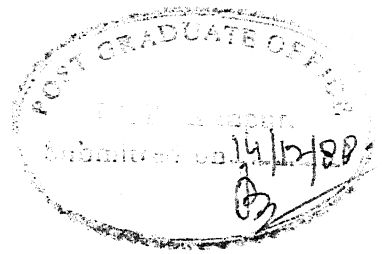## MASTER OF TECHNOLOGY

by

SUSHIL K. SRIVASTAV

to the

DEPARTMENT OF CIVIL ENGINEERING
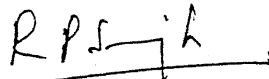
INDIAN INSTITUTE OF TECHNOLOGY, KANPUR

DECEMBER, 1988

CE-1900-M-SRI-MIC

CERTIFICATE

This is to certify that the present work entitled, "MICROWAVE REMOTE SENSING RESPONSE OF SNOW COVERED TERRAINS", being submitted by Mr. Sushil K. Srivastav in partial fulfilment of the requirements for the degree of M.Tech., is a record of his own work carried out by him under my supervision and guidance. The matter embodied in this thesis has not been submitted elsewhere for the award of a degree or diploma.

Dated : 14th December, 1988

(Ramesh P. Singh)
Assistant Professor
Deptt. of Civil Engineering
Indian Institute of Technology
Kanpur- 208 016, INDIA

ACKNOWLEDGEMENT

Dated : 14th December, 1988   (Sushil K. Srivastav)

DEDICATED

TO

THOSE STRIVING TO CONSERVE RATHER CONSUME

CONTENTS

ABSTRACT

Almost whole of the year, mid- to high-lattitude regions are covered with snow. The snowpack undergoes several cycles of melting and refreezing throughout the year, which influences the weather conditions, and surface and subsurface water. The capability of microwaves to penetrate snow layer and respond to variations in subsurface properties along with all-weather and all-time observational capabilities make Microwave Remote Sensing an useful tool to monitor snowpack properties on global scale. The microwave portion of electromagnetic spectrum is advantageous additionally because of the large difference in the dielectric constant of liquid and frozen water, which causes a strong variation in the observed microwave signal when liquid water is present.

In order to study the microwave remote sensing response over snow covered areas, detailed numerical calculations have been carried out over various two-layered and multi-layered models representative of such areas. The results show that the microwave remote sensing can be used to map the snow cover extent, to classify snow types, to estimate snow thickness, to detect onset of snowmelt, to estimate the free liquid water content of snow, to monitor the roughness of snow surfaces, and to estimate the lake ice thickness. The detailed discussion of the results have been presented in view of the proper selection of operating parameters of microwave remote sensors for the mapping of snow covered regions.

CHAPTER 1

INTRODUCTION

1.1 GENERAL VIEW

The volume of ice and snow on earth is enormous: enough to cover its entire surface with a layer roughly 60 meter thick. Roughly 50 percent of earth's surface is, at present, covered by snow or ice during most of the year. Ice is not uniformly distributed over the earth but is instead concentrated in the polar regions and mountains, attaining thicknesses of over 4,000 meters; snow is concentrated in mid - to high - lattitude regions (EOS, V.II f). Figure 1.1 shows the sea ice, glaciers and snow regimes for the northern and southern hemisphere.

Snow after being deposited on earth's surface serves as a source of water vapour input to the atmosphere through the processes of sublimation and evaporation and also as a source of water to the soil and river systems after its melting. With the increasing demand for water throughout the world, effective management of the water resources is required in order to predict and distribute the available water supply efficiently.

The use of remote sensing techniques offer an outstanding opportunity to survey the snow cover much more extensively than can be done practically from the ground, since snow fields normally occur in remote and inaccessible areas where the data collection becomes very difficult and hazardous.
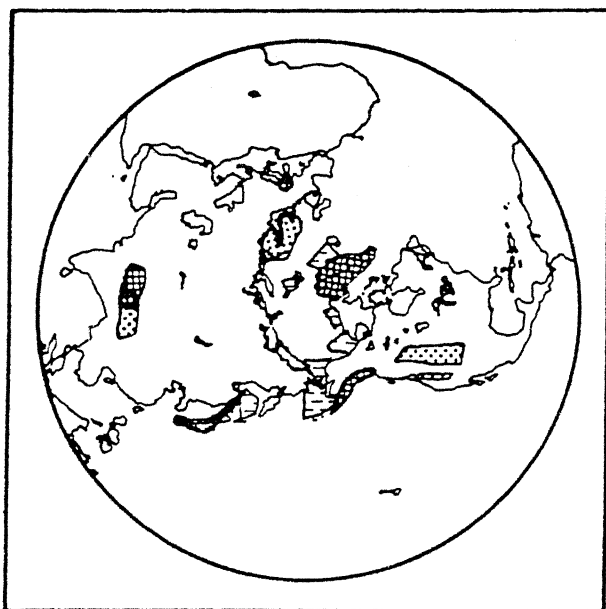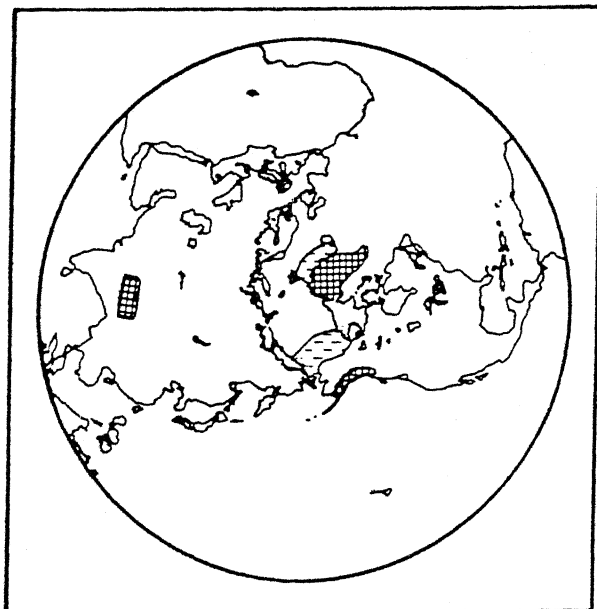
WINTER   SUMMER

NORTHERN HEMISPHERE
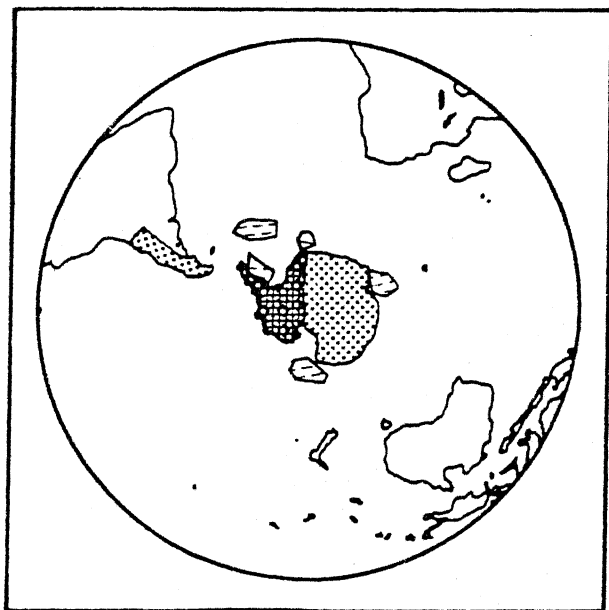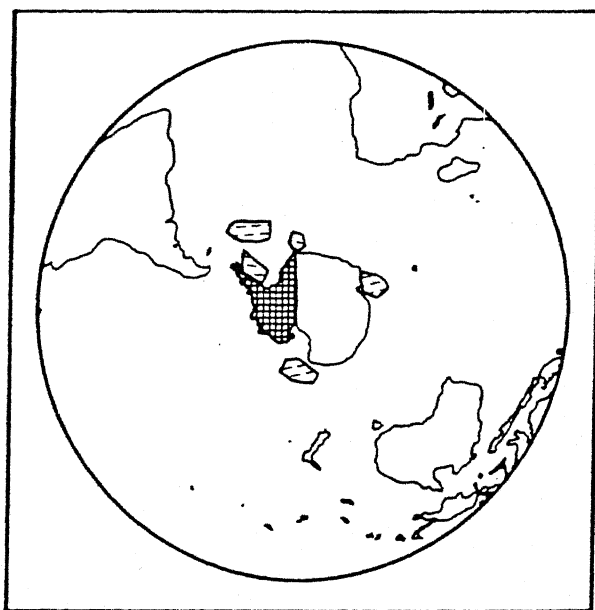
WINTER   SUMMER

SOUTHERN HEMISPHERE

KEY

SEA ICE
GLACIERS
SNOW

Fig. 1.1. Sea ice, glaciers and snow regimes for the northern and southern hemisphere (EOS, v. II f).

1.2 DEFINITION AND CONCEPT OF REMOTE SENSING

Remote sensing is the technique of obtaining information about an object, area, or phenomenon through the analysis of data acquired by a device that is not in contact with the object, area, or phenomenon under investigation. Remote sensing is possible in three regions of electromagnetic spectrum (Figure 1.2) namely, visible and near infra-red, thermal infra-red and microwave. The two basic processes involved are 'data acquisition' and 'data analysis'. The elements of the data acquisition process are :

(a)   energy sources,

(b)   propagation of energy through the atmosphere,

(c)   energy interactions with earth surface features,

(d)   re-transmission of energy through the atmosphere,

(e)   air borne and/or spaceborne sensors, and

(f)   generation of sensor data in pictorial and digital form.

The data analysis process involves examining the pictorial and digital sensor data. In short, we use sensors to record variations in the way earth surface features reflect and emit electromagnetic energy, which is used further to deduce the surface and subsurface information.

1.3 WHY MICROWAVES FOR REMOTE SENSING ?

The microwave portion of electromagnetic spectrum extends from 0.3 to 300 GHz range of frequency (1 mm to 1m range of wavelength). The microwave region is further classified in various

frequency (cycles/second)

10^{18} 10^{16} 10^{14} 10^{12} 10^{10}

| X rays | ultra-violet | visible | near | infrared: medium and far | microwave |

wavelength

ĩ00 Å   4000 Å   7000 Å   15000 Å   1mm

Scanners with
filtered photo-
multipliers;
cameras
with filtered
infrared film;
lasers

film in cameras

cameras with
infrared sensitive
film; solid-state
detectors in
scanners and
radiometers

solid-state
detectors
in scanners and
radiometers

radar;
receivers in
scanners and
radiometers

Fig. 1.2   The electro-magnetic spectrum (Carter, 1986).

bands of narrow frequency range and is shown in Table1.1 (Ulaby et al., 1981). Remote sensing by microwaves has additional advantages over the visible and near infra-red and thermal infra-red regions of electromagnetic spectrum because -

(a)   microwaves have capability to penetrate clouds and to some extent rain, i.e., all-weather observation is possible,

(b)   microwave sensors have capability to probe the target day and night, and

(c)   microwaves have capability to penetrate deeper into the target and consequently information with depth is available, whereas in visible and infra-red region only surface information is known.

1.4 OBJECTIVES OF THE STUDY

In developing countries like ours, monitoring of snow and ice cover is very important in water resources development and management. By knowing the physical parameters of snowpack, an accurate estimate of annual runoff of major rivers due to melting of glaciers (almost all the rivers in northern part of India) can be predicted, that will aid the effective management of water resources to distribute the available water supply in domestic, irrigational and industrial sectors.

The present study was carried out with the following objectives :

(i)   to relate the dielectric constant of snow with frequency, density of snow, liquid water content and physical temperature of the snowpack,

TABLE 1.1. Band designations in the microwave region

Band	Frequency Range (GHz)
P	0.225 - 0.39
L	0.390 - 1.55
S	1.550 - 4.20
C	4.200 - 5.75
X	5.750 - 10.9
K	10.90 - 36.0
Q	36.00 - 46.0
V	46.00 - 56.0
W	56.00 - 100.0

(ii)   to estimate the scattering, absorption, and extinction losses of electromagnetic energy and penetration depth of microwave signal in the snowpack,

(iii)   to discriminate snow covered areas from bare ground surfaces,

(iv)   to classify snow types,

(v)   to estimate snow thickness for the determination of snow water equivalent,

(vi)   to estimate the liquid water content of snow,

(vii)   to study the effect of roughness of snow surfaces caused due to snow melting and local winds on microwave remote sensing response,

(viii)   to study the behaviour of microwave signals over natural lake or river ice (in case of pure and saline water),

(ix)   to study the effect of incidence angle, polarization (both horizontal and vertical) and frequency on reflectivity, emissivity and brightness temperature of snow and ice covered surfaces, and

(x)   to suggest ultimately, the optimum sensor parameters for remote sensing of snow and ice cover.

1.5 ORGANIZATION OF THE STUDY

Besides this introductory chapter, the thesis contains four more chapters, covering the whole aspects of microwave remote sensing to monitor snow and ice cover on the surface of the earth. Chapter II describes the general theory of passive microwave remote sensing systems. A detailed discussion of

emission behaviour of two-layered and multi-layered snow and ice surfaces has been dealt here. The effect of surface roughness on reflectivity caused due to local features like strong katabatic winds and snow melting is also discussed here. Chapter III deals with the physical properties of snow and ice as wall as various algorithms to calculate the dielectric constant of snow, ice and water. The behaviour of real and imaginary parts of dielectric constants of dry and wet snow with the frequency of microwave signal, snow density, liquid water content of snow and surface temperature has also been discussed in this chapter. In chapter IV, we have presented the microwave remote sensing response over various layered models representative of snow covered terrains. Conclusions and further recommendations are given in Chapter V.

The Computer programs developed and used in the present study are appended at the end.

CHAPTER 2

THEORY OF MICROWAVE REMOTE SENSING

2.1 INTRODUCTION

All-weather and all-time observational capabilities and deeper penetration into the ground make microwave sensors more advantageous over visible and infrared sensors. In microwave remote sensing the microwave response (scattered or emitted energy) is controlled by the target as well as sensor parameters. Target parameters include- i) surface geometry, ii) subsurface geometry, and iii) dielectric properties of the surface and subsurface material; and sensor parameters include i) wavelength or frequency of electromagnetic radiation, ii) polarization, iii) angle of observation, and iv) spatial resolution. The fundamentals of microwave remote sensing systems as an overview and various formulae to compute the brightness temperature over two-layered and multi-layered models are given in this chapter.

2.2 MICROWAVE REMOTE SENSING SYSTEMS

The microwave remote sensing systems are classified into two categories viz. Passive and Active, based on the source of electromagnetic energy. The systems which detect the emitted microwave radiation by the target are called passive systems, e.g., microwave radiometers. The systems which transmit the microwave radiation to illuminate the target and at the same

time receive the return or back scattered signal are called active microwave remote sensing systems, e.g., scatterometers, altimeters, side looking airborne radar (SLAR) and synthetic aperture radar (SAR) etc.

The microwave remote sensing systems can also be classified as non-imaging and imaging sensors. The examples of non-imaging sensors are radiometers in non-scanning mode, scatterometer, altimeter etc. and are very useful for understanding the physical phenomenon and modelling purposes. In the case of imaging sensors, the information is gathered and the results are depicted in two-dimensional pictorial form known as images. The radiometers in the scanning mode, side looking airborne radar (SLAR) and synthetic aperture radar (SAR) are some of the the examples of imaging sensors. These sensors produce the image of the object, which is useful for the detection and assessment of natural resources.

2.3 PASSIVE MICROWAVE REMOTE SENSING

A microwave radiometer like other passive electromagnetic sensors measures the emitted energy from the targets within the field of view of its antenna. This emitted energy is quantified in terms of brightness temperature (T_B) which is a well defined function of electrical property, i.e., dielectric constant of the medium under investigation and also of physical temperature of the object.

2.3.1 Derivation of Brightness Temperature

According to Planck's quantum theory of black body

radiation, all the objects above $0^{\circ}K$ radiate electromagnetic energy. The mathematical formula given by Planck is

$$B_f = \frac{2hf^3}{c^2 \ [\ \exp(hf/kT) - 1\ ]} \ , \qquad (2.1)$$

where

B_f is the blackbody spectral brightness, $W\ m^{-2}\ Sr^{-1}\ Hz^{-1}$,

h is the Planck's constant, $6.63 * 10^{-34}$ J-sec,

f is the frequency in Hz,

k is Boltzmann constant, 1.38×10^{-23} J/K,

T is absolute surface temperature in $^{\circ}K$,

c is the velocity of light, 3×10^8 m/sec.

In microwave region, hf/KT $<<$ 1 (Rayleigh - Jean's law). Therefore, the Planck's formula reduces to

$$B_f = \frac{2\ f^2}{c^2}\ k\ T \ . \qquad (2.2)$$

All the materials, referred to as grey bodies emit less than a black body does and do not necessarily absorb all energy incident upon it, so

$$B_f' = \frac{2\ f^2}{c^2}\ k\ T_B \ , \qquad (2.3)$$

where B_f' is the spectral brightness of grey body. The emissivity is defined as the ratio of the spectral brightness of the grey body to that of the black body. Therefore,

$$e = \frac{B_f'}{B_f} = \frac{T_B}{T} \qquad (2.4)$$

or $\qquad T_B = e \cdot T$, $\hspace{6cm}$ (2.5)

where e is referred to as emissivity of the medium and varies
between zero and one $(0 < e < 1)$. Emissivity of a material
depends upon frequency, polarization, incidence angle, complex
dielectric constant, surface temperature and surface roughness.

2.3.2 Brightness Temperature (T_B) Recorded by Radiometers

In general, the radiation received by an airborne
or spaceborne radiometer can be split into three components: the
first is the self-emission from the surface of the object, the
second is the reflection at the surface of the downwelling
radiation from the atmosphere, and the third is the upwelling
radiation of the atmosphere directly incident upon the radiometer
(Figure 2.1). If the intervening atmosphere is lossy, the
radiations emanating from the object will be attenuated and the
lossy atmosphere itself will emit thermal radiation. Thus
brightness temperature of the object can be written as

$$T_B = \tau (r \, T_{sky} + (1 - r) \, T_{surf}) + T_{atmos} , \hspace{1cm} (2.6)$$

where r is the surface reflectivity and τ is the atmospheric
transmissivity. The first term in the equation (2.6) is the
reflected sky brightness temperature which depends on the
wavelength and atmospheric conditions, the second term is the
emission from the surface of the object and the third is the
contribution from the atmosphere between the surface and the
receiver.
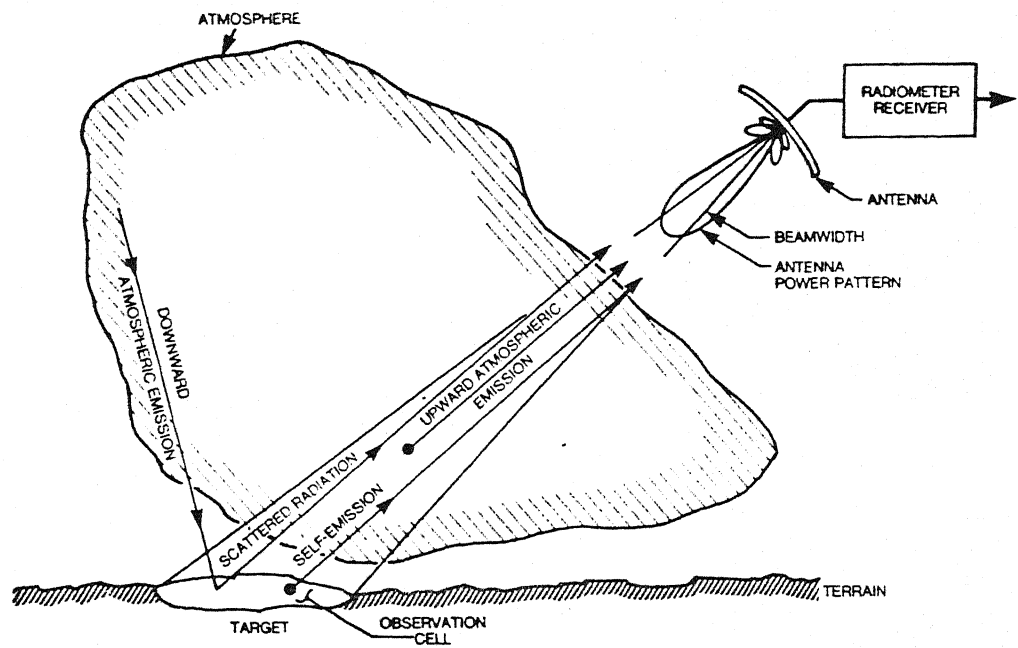
Fig. 2.1. Contribution of radiation from the surface and the atmosphere, received by an airborne and spaceborne sensor (Foster et al., 1984).
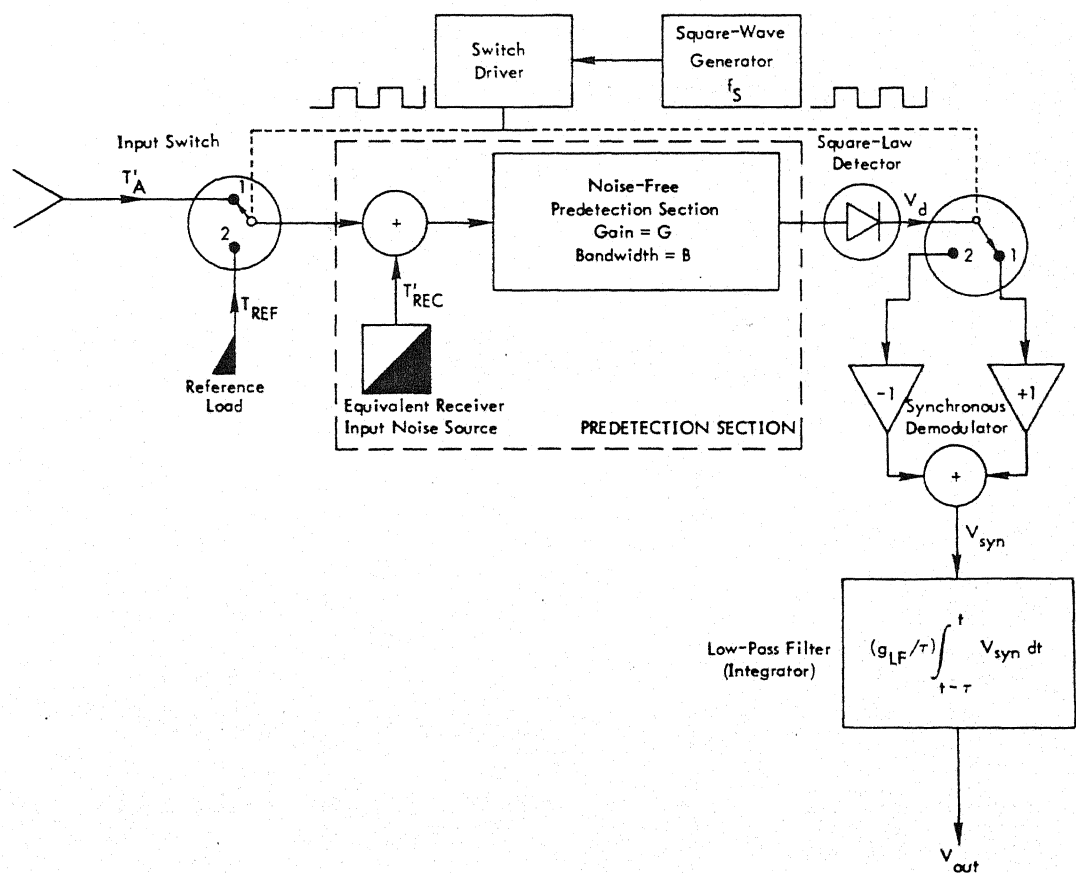
Fig. 2.2. Block diagram of the Dicke radiometer (Ulaby et al., 1981).

13

2.3.3 Radiometers

A radiometer is merely a passive receiver which records self-emitted and/or reflected radiation by the scene. Most of the microwave radiometers are Dicke type of radiometers. A block diagram of the Dicke radiometer is shown in Figure 2.2 (Ulaby et al.,1981). It consists of basically high gain antenna, a Dicke switch, a noise source, predetection section, square-law detector, synchronous demodulator placed in between the square-law detector and the low-pass filter (integrator). The predetection section consists of the RF amplifier, mixer, and IF amplifier and is characterized by a power gain (G) and bandwidth (B). Dicke switch, connected at the receiver input (at a point as close to the antenna as possible) is used to modulate the receiver input signal. The radiometer output is in millivolts. Calibration of radiometer gives the temperature corresponding to radiometer output voltage.

2.3.4 Resolution and Limitations

Two of the most important parameters of the radiometer are the ground resolution and measurement accuracy. The specified temperature measurement accuracy of presently available radiometer is 0.1 $^{\circ}$K. The ground resolution of microwave radiometer depends upon the height of the platform and on the beamwidth of the radiometer antenna. From a platform flying at an altitude H, the linear extent of resolution will be

$$r = H \cdot \phi_B = 1.2 \frac{\lambda}{D} H , \qquad (2.7)$$

where

    ϕ_B is the antenna beamwidth,

    λ is the wavelength of the receiving radiation, and

    D is the diameter of the antenna aperture.

From the above equation, it is clear that for a practical antenna size, the achievable ground resolution from the satellite height is poor.

2.4 SNOW PARAMETERS AND SENSOR RESPONSES

Table 2.1 shows the snow parameters affecting measured response by various sensors. As shown in table, water equivalent is the key property for gamma ray sensors, albedo (the ratio of reflected to incoming solar radiation) is most important for visible and near infra-red sensors, emissivity is most meaningful for the thermal infra-red sensors, and the dielectric constant is most significant for microwave sensors.

Microwaves have the capability to penetrate snow and respond to variations in subsurface properties. The microwave sensors have potential to monitor many important snowpack properties such as depth, water equivalent, presence of melting, and the state of underlying ground because emitted, reflected and scattered electromagnetic radiations from the snowpack are sensitive to changes in snowpack properties (Foster et al., 1984).

2.5 MODEL PARAMETERS OF SNOW

The absorption and scattering coefficients are the model parameters (also known as propagation parameters), used to

TABLE 2.1. Snow parameters affecting sensor responses

Gamma Ray Sensors

- snow depth

- background radiation

Visible/Near-Infrared (Albedo) Sensors

- crystal size

- contaminants

- snow depth (only for shallow snow, i.e. upto

  a few centimeters)

- liquid water

- surface roughness

Thermal Infrared Sensors

- temperature

- crystal size

- liquid water

Microwave Sensors

- liquid water

- crystal size

- water equivalent depth

- stratification

- snow surface roughness

- density

- temperature

- soil condition

compute the emission from a snow layer. The sum of the absorption (k_a) and scattering coefficients (k_s) is known as the extinction coefficient (k_e), which is related as (ulaby et al., 1986)

$$k_e = k_s + k_a . \tag{2.8}$$

The albedo (a) of the snow medium is defined as

$$a = k_s / k_e . \tag{2.9}$$

Scattering of microwave signals in snow is mainly due to the presence of ice particles, therefore, scattering coefficient is the sum of the scattering cross-sections of all the ice spheres contained in a unit volume, expressed as

$$k_s = \sum_{j=1}^{N_v} Q_s (r_j, n) , \tag{2.10}$$

where N_v is the number density of ice spheres. The absorption coefficient of snow consists of two contributions: i) absorption by ice spheres (k_{ai}), and ii) absorption by the background medium (k_{ab}). Therefore

$$k_a = k_{ai} + k_{ab} , \tag{2.11}$$

where

$$k_{ai} = \sum_{j=1}^{N_v} Q_a (r_j, n) , \tag{2.12}$$

and

$$k_{ab} = 2k_0 (1-v_i) n_b^{''} ,$$
$$= 2k_0 (1-v_i) |Im (\varepsilon_b)| . \tag{2.13}$$

In the above equations, k_0 is the wave number in free space, v_i is the volume fraction of ice particles in the mixture,

$n_b^{''}$ is the imaginary part of complex index of refraction of the background medium, and ε_b is the complex dielectric constant of the background medium. The wave number (k_0) and volume fraction of ice particles (v_i) are given by

$$k_0 = 2\pi / \lambda_0 , \qquad (2.14)$$

$$v_i = \rho_s / \rho_i , \qquad (2.15)$$

where ρ_s and ρ_i are the density of snow and ice respectively. For dry snow, the background medium is air and $n_b^{''} = 0.0$, hence $k_a = k_{ai}$. For wet snow, k_{ab} can be estimated by equation (2.13). The Rayleigh expressions $Q_a(r_j,n)$ and $Q_s(r_j,n)$ for an ice particle of radius r_j are given by (Ulaby et al., 1981)

$$Q_a(r_j,n) = \frac{8\,\pi^2}{\lambda_b}\, r_j^3 \; \text{Im}\,(\,-K\,) , \qquad (2.16)$$

and

$$Q_s(r_j,n) = \frac{128\,\pi^5}{3\,\lambda_b^4}\, r_j^6 \; |K|^2 , \qquad (2.17)$$

where

$$K = \frac{\varepsilon - 1}{\varepsilon + 2} , \qquad (2.18)$$

and

$$\varepsilon = \varepsilon_i / \varepsilon_b . \qquad (2.19)$$

In the above equations, ε_i and ε_b are the complex dielectric constant of ice and background medium respectively. From equations (2.10) and (2.12), we can write

$$k_s = \frac{128\,\pi^5}{3\,\lambda_b^4}\, |K|^2 \sum_{j=1}^{N_v} r_j^6 , \qquad (2.20)$$

$$k_{ai} = \frac{8\pi^2}{\lambda_b} \text{Im}(-K) \sum_{j=1}^{N_v} r_j^3 . \qquad (2.21)$$

If the mean or typical radius of ice particles is r and all the particles are assumed to be of the same size, then the number density of ice particles is given by

$$N_v = \frac{\rho_s}{\rho_i} \left[\frac{4}{3}\pi r^3 \right]^{-1} . \qquad (2.22)$$

In wet snow, background medium consists of air and water. In the present calculations water droplets are assumed to be spherical and air as the host dielectric material, then the dielectric constant of the background medium can be represented by Polder-Van Santen two-phase mixing formula (Ulaby et al., 1986)

$$\varepsilon_b = 1 + \frac{m_v}{3}(\varepsilon_w - 1) \sum_{u=a,b,c} \left[\frac{1}{1 + A_u(\varepsilon_w/\varepsilon_b - 1)} \right] , \qquad (2.23)$$

where m_v is the volumetric water content of snow, ε_w is the dielectric constant of water, and A_a, A_b and A_c are the depolarization factors of spherical water droplets (= 1/3). On solving, equation (2.23) simplifies to

$$2\varepsilon_b^2 + \varepsilon_b((\varepsilon_w-1)(1-3m_v) - 1) - \varepsilon_w = 0 , \qquad (2.24)$$

which is a simple quadratic equation that can be solved to determine the dielectric constant of the background medium. Since ice is a scatter-free medium, therefore total loss of electromagnetic energy is only due to absorption which is expressed

as -

$$k_a = k_0 (\varepsilon_i'' / \sqrt{\varepsilon_i'}) , \tag{2.25}$$

where ε_i' and ε_i'' are the real and imaginary parts of complex dielectric constant of pure ice. The penetration depth (δ_p) of microwave signal in a scattering medium (like snow) is given by

$$\delta_p = 1 / k_e , \tag{2.26}$$

where k_e is the extinction coefficient of snow layer.

2.6 APPROACH TO COMPUTE BRIGHTNESS TEMPERATURE

In passive microwave remote sensing, basically two approaches are possible: the first is the non-coherent approach in which the theory is developed considering the basis of electromagnetic intensity, and second is the coherent approach in which electromagnetic field is considered. In the present work, brightness temperature has been computed using non-coherent approach given by Ulaby et al. (1981) for two-layered case (as shown in Figure 2.3). The brightness temperature (T_B) at a point above the boundary between air and a medium consisting of two layers can be determined by the following expression -

$$T_B = \frac{1 - r_1}{\left(1 - \frac{r_1 r_2}{L^2}\right)} \left[\left[\left(1 + \frac{r_2}{L}\right)\left(1 - \frac{1}{L}\right)\left(1 - a\right) T_1 + \left(\frac{1 - r_2}{L}\right) T_2 \right] \right] , \tag{2.27}$$

where r_1 and r_2 are the Fresnel's reflectivities at the two interfaces, L and a are the loss factor and albedo of the second layer respectively, and T_1 and T_2 are the average temperatures of the layer 1 and 2 respectively. The loss factor of the first layer

air

$\epsilon_1 = 1$
$\mu_1 = 1$

θ_1 θ_1

Boundary 1
Layer 1

θ_2

d

ϵ_2
μ_2

θ_2 θ_2

Boundary 2
Layer 2

ϵ_3
μ_3

θ_3
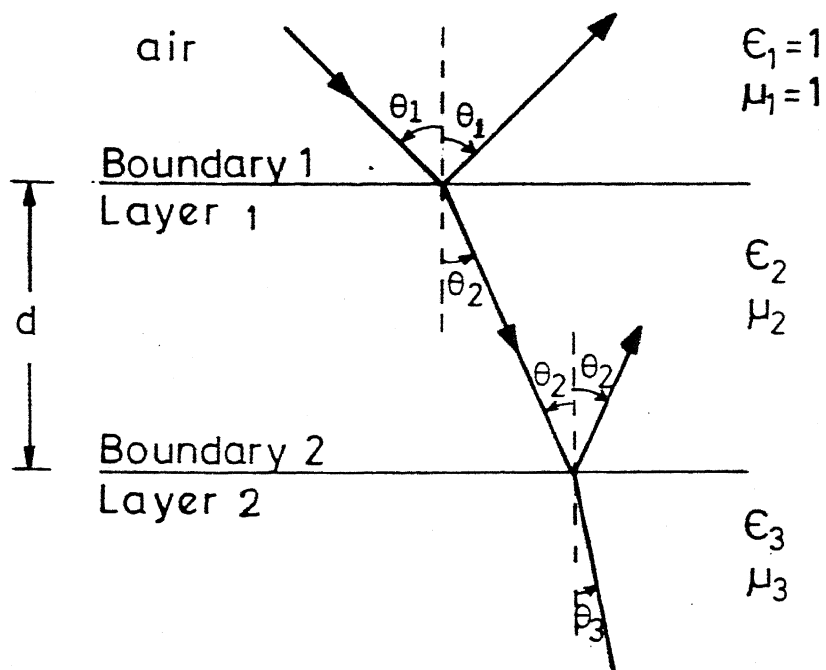
Fig. 2.3. Geometry of the two-layered model.

is given by -

$$L = \exp(k_e \, d \, \sec \theta_2),\hspace{3cm}(2.28)$$

where θ_2, k_e and d represent the refraction angle, extinction coefficient and thickness of the layer 1 respectively. If the average physical temperature of the layer 1 and 2 are assumed to be the same ($T_1 = T_2 = T$), equation (2.26) reduces to

$$T_B = e \cdot T,\hspace{4cm}(2.29)$$

where e is the incoherent emissivity and can be represented as -

$$e = \frac{(1 - r_1)}{\left[1 - \dfrac{r_1 \, r_2}{L^2}\right]} \left[\left[\left(1 + \frac{r_2}{L}\right)\left(1 - \frac{1}{L}\right)\left(1 - a\right) + \left(\frac{1 - r_2}{L}\right)\right]\right].\hspace{1cm}(2.30)$$

The normalized impedances of the three media are given by the following expression -

$$Z_i = \begin{cases} \eta_i \cos \theta_i, & \text{for vertical polarization} \\ \eta_i \sec \theta_i, & \text{for horizontal polarization} \end{cases},\hspace{1cm}(2.31)$$

where

$$\eta_i = \sqrt{\mu_i / \varepsilon_i},\hspace{4cm}(2.32)$$

and $\qquad i = 1, 2, 3.$

Here, μ_i and ε_i denote the relative permeability and relative complex dielectric constant of the respective medium. The refraction angles θ_2 and θ_3 can be determined by using Snell's law. The reflectivity at the two interfaces is given by -

$$r_1 = |(Z_2 - Z_1) / (Z_2 + Z_1)|^2, \text{ and}\hspace{2cm}(2.33)$$

$$r_2 = |(Z_3 - Z_2) / (Z_3 + Z_2)|^2.\hspace{2.5cm}(2.34)$$

As discussed in the next chapter, snow is deposited in discrete layers and the characteristics of one layer differ from another, i.e., snowpack parameters vary with depth. The dielectric constant also varies accordingly, which affects the emission behaviour of the snowpack. The brightness temperature for multi-layered case can be computed in the similar manner. The formulation discussed above was used to study the behaviour of brightness temperature over two-layered and multi-layered snow models.

2.7 EFFECT OF SURFACE ROUGHNESS

The polar and mid- to high-lattitude regions are surrounded by low pressure and the surface topography of the snow and ice surfaces are often disturbed due to the presence of snow melting and strong katabatic winds. The microwave signals incident upon these disturbed surfaces are partly reflected in the specular direction and partly scattered in all directins. In order to study the effect of surface roughness on reflectivity, we have used the following semi-empirical relation (Choudhury et al., 1979)

$$ r = r^{sp} e^{-h'} \cos^2 \theta , \qquad (2.35) $$

where r^{sp} is the specular surface reflectivity, θ is the angle of incidence and h' is surface roughness parameter given by -

$$ h' = 4 k_0^2 \sigma^2 , \qquad (2.36) $$

where k_0 is the wave number in free space and σ is the surface height variation.

CHAPTER 3

PHYSICAL AND DIELECTRIC PROPERTIES OF SNOW AND ICE

3.1 INTRODUCTION

The electromagnetic properties of a snowpack vary as its structure and composition change. As discussed in the previous chapter, microwave sensor response is highly dependent upon physical and dielectric properties of a snowpack. An accurate analysis of the microwave remote sensing data requires prior knowledge of physical and dielectric properties of water, snow, ice and other geologic materials (Singh, 1984). In the following sections physical and dielectric properties of snow and ice, and empirical relations for calculating the dielectric constant of water (both pure and saline) and bare ground are discussed.

3.2 PHYSICAL PROPERTIES OF SNOW AND ICE

In areas where annual snowfall exceeds the loss of snow due to melting, a layer of snow gets accumulated every year. The yearly accumulation of snow acquire immense size and shape. The newly fallen snow, which is extremely light and highly porous mass of frozen water and air, undergoes a series of changes with time. It is first compacted to a granular mass of almost spherical grains with specific gravity increasing from as low as 0.05 to 0.50 and porosity reducing from original 95 percent to 50 percent or

less.   This is the firn or ne've', a variety of ice. With continued compaction due to increasing mass of snow layers from above, firn undergoes further changes towards a very compact, dense, coarsely crystalline mass with a specific gravity of 0.916 and with little or no porosity, defined as ice.

Snow is a fine grained material with a large specific area. The shape and size of the snow particles change very rapidly during melting and refreezing cycles, especially in response to changing weather conditions. The snowpack properties vary throughout the life history of a snow cover and since snow is deposited in discrete layers, the pack may vary throughout its depth. Moreover, the effects of wind and local melting can create horizontal inhomogeneity. This variability makes monitoring snowpacks all the more challenging and crucial (Foster et al., 1984).

Fresh, dry snowflakes display crystal facets because they grow rapidly in the atmosphere. The flakes metamorphose, either via destructive metamorphism to rounded grains or via constructive metamorphism to large, faceted crystals known as depth hoar.

Equilibrium thermodynamics favours destructive metamorphism, which controls the shape of the small, well rounded grains that generally dominate a dry snow cover. But when there is a steep temperature gradient, constructive metamorphism occurs, and large, angular, and hollow crystals of depth hoar grow in the warmer layers at the base of the snowpack (Foster et al., 1984).

When snow is wet, its structure and its

electromagnetic behaviour change markedly. Two geometrics of wet snow are common: freely draining snow with low liquid water content (2-6% by volume) and snow with a high liquid water content where water flow is impeded. The grain size increases rapidly following even slight wetting. At higher liquid water contents, the grains grow at the faster rate than in freely draining snow. This type of snow is cohesionless, with well rounded grains about 1 mm in radius, and fully surrounded by water. (Colbeck, 1982).

3.3 EQUATIONS FOR CALCULATING DIELECTRIC CONSTANT OF ICE, SNOW, WATER AND BARE GROUND

In microwave remote sensing, knowledge of the dielectric properties of the materials is important for the interpretation of the microwave reflection or emission data (Singh, 1984). The dielectric properties of the materials are characterized by its relative complex dielectric constant (ε_r^*) and loss tangent (tan δ_s), where the subscripts r and s refer to relative and snow respectively. However, for simplicity the use of the term relative and hence the subscript r is avoided in the forthcoming discussions. The dielectric constant (ε^*) is a measure of the response of the material to an applied electromagnetic field. This response can be split into two factors: the first determines the propagation characteristics of the wave in the material, i.e., velocity and wavelength, and the second is a measure of the energy losses in the media. These two factors are represented by the real (ε') and imaginary (ε'') parts of the complex dielectric constant. The ratio $\varepsilon'' / \varepsilon'$ is called the loss tangent (tan δ_s) for

the material.

$$\varepsilon^* = \varepsilon' - i\varepsilon'' \qquad (3.1)$$

$$\tan \delta_s = \varepsilon'' / \varepsilon' \qquad (3.2)$$

where $i = \sqrt{-1}$, ε' is referred to as the dielectric permittivity of the medium and ε'' is known as the dielectric loss factor of the medium. In general, the values of ε' and ε'' are functions of frequency and temperature both.

The equations for calculating the dielectric constant of pure ice, saline ice, snow, pure water, saline water and bare ground have been discussed in the following sections :-

3.3.1 Dielectric Constant of Pure Ice

The real part of complex dielectric constant of pure ice (ε_i') is independent of both temperature and frequency in the microwave region, and is assigned the constant value

$$\varepsilon_i' = 3.15 , \qquad (3.3)$$

however, the imaginary part (ε_i'') exhibits strong variations with both parameters. Values of ε_i'' are taken for the calculation of dielectric constant of snow and saline ice as shown in Figure 3.1 at -1 and -20°C (Stiles et al., 1981). The subscripts i refers to pure ice.

3.3.2 Dielectric Constant of Saline Ice

Saline ice is a much more complicated medium, both structurally and electromagnetically than fresh-water ice and is a heterogeneous mixture of liquid-brine inclusions and air pockets interspersed within the ice medium. The brine inclusions,

27
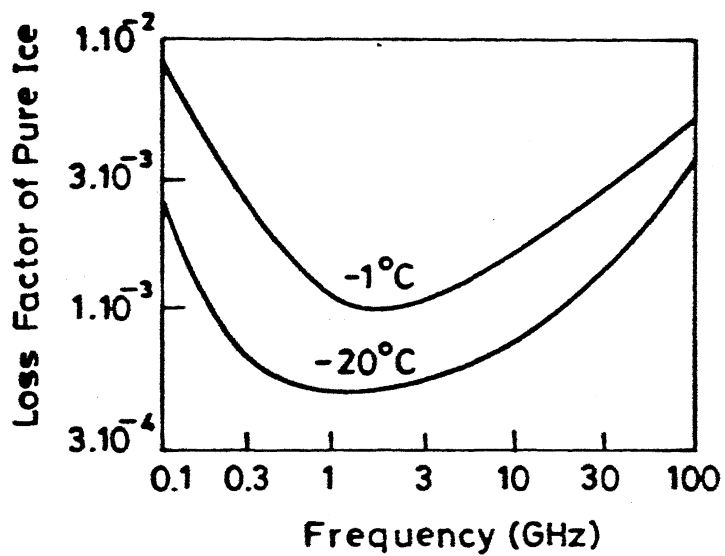
Fig. 3.1. The imaginary part of complex dielectric constant (ε_i'') of pure ice.

containing salt and water, show strong influence on the complex dielectric constant of the materials (Rankin and Singh, 1985, and Singh et al., 1989) because of their high complex dielectric constant when compared to that of ice.

In general, the complex dielectric constant of saline ice (ε_{si}) is a function of the following parameters –

(a) the complex dielectric constant of pure ice (ε_i),

(b) the complex dielectric constant of the brine pockets or inclusions (ε_b),

(c) the fraction of brine by volume (v_b), and

(d) the shape and orientation of the brine pockets or inclusions.

The salinity of liquid brine (S_b) is governed by its temperature and can be calculated by the following empirical expressions (Assur, 1960 ; Poe et al., 1972) –

$$S_b = 1.725 - 18.756\ T - 0.3964\ T^2\ , \quad -8.2 \leq T \leq -20\ ^\circ C \quad (3.4)$$

$$S_b = 57.041 - 9.929\ T - 0.1620\ T^2 - 0.002396\ T^3\ ,$$
$$-22.9 \leq T \leq -8.20\ ^\circ C \quad (3.5)$$

$$S_b = 242.94 + 1.5299\ T + 0.0429\ T^2\ , \quad -36.8 \leq T \leq -22.9^\circ\ C$$
$$(3.6)$$

$$S_b = 508.18 + 14.535\ T + 0.2018\ T^2\ , \quad -43.2 \leq T \leq -36.8^\circ\ C$$
$$(3.7)$$

The salinity of liquid brine (S_b), is related to normality (N_b) by (Klein and Swift, 1977)

$$N_b = S_b\ [1.707 \times 10^{-2} + 1.205 \times 10^{-5}\ S_b + 4.058 \times 10^{-9}\ S_b^2\ ],$$
$$(3.8)$$

and ε_b' and ε_b'' for pure NaCl solution are given by Stogryn's

(1971) formulation as

$$\varepsilon_b' = \varepsilon_{w\infty} + \frac{\varepsilon_{b0} - \varepsilon_{w\infty}}{1 + (2\pi f \tau_b)^2} \quad , \tag{3.9}$$

$$\varepsilon_b'' = (2\pi f \tau_b) \frac{\varepsilon_{b0} - \varepsilon_{w\infty}}{(1 + 2\pi f \tau_b)^2} + \frac{\sigma_b}{2\pi f \varepsilon_0} \quad , \tag{3.10}$$

where $\varepsilon_{w\infty} = 4.9$, and

$$\varepsilon_{b0}(T,N_b) = \varepsilon_{b0}(T,0) \, a_1(N_b) \, , \tag{3.11}$$

$$\tau_b(T,N_b) = \tau_b(T,0) \, b_1(T,N_b) \, , \tag{3.12}$$

$$\sigma_b(T,N_b) = \sigma_b(25,N_b) \, C_1(\Delta,N_b) \, . \tag{3.13}$$

The above functions are given by the following expressions -

$$\varepsilon_{b0}(T,0) = 88.045 - 0.4147\, T + 6.295 \times 10^{-4}\, T^2$$
$$+ 1.075 \times 10^{-5}\, T^3 \, , \tag{3.14}$$

$$a_1(N_b) = 1.0 - 0.255\, N_b + 5.15 \times 10^{-2}\, N_b^2 - 6.89 \times 10^{-3}\, N_b^3 \, , \tag{3.15}$$

$$\tau_b(T,0) = (1.1109 \times 10^{-10} - 3.824 \times 10^{-12}\, T + 6.938 \times 10^{-14} T^2$$
$$- 5.096 \times 10^{-16}\, T^3) \, / \, 2\pi \, , \tag{3.16}$$

$$b_1(T,N_b) = 1.0 + 0.146 \times 10^{-2}\, T\, N_b - 4.89 \times 10^{-2}\, N_b$$
$$- 2.97 \times 10^{-2}\, N_b^2 + 5.64 \times 10^{-3}\, N_b^3 \, , \tag{3.17}$$

$$\sigma_b(25,N_b) = N_b(10.39 - 2.378\, N_b + 0.683\, N_b^2 - 0.135\, N_b^3$$
$$+ 1.01 \times 10^{-2}\, N_b^4) \, , \tag{3.18}$$

$$c_1(\Delta,N_b) = 1.0 - 1.96 \times 10^{-2} + 8.08 \times 10^{-5} \Delta^2 - N_b[3.02 \times$$
$$10^{-5} + 3.92 \times 10^{-5} + N_b(1.72 \times 10^{-5}$$
$$- 6.58 \times 10^{-6})] \, , \tag{3.19}$$

where T is in $^{\circ}C$ and $\triangle = (25 - T)$.

The following empirical relations given by Frankenstein and Garner (1967) can be used to compute the volume fraction of brine in Saline ice -

$$v_b = 10^{-3} S_{si}(-\frac{52.56}{T} - 2.28) , \qquad -0.5 \geq T \geq -2.06 \ ^{\circ}C \tag{3.20}$$

$$v_b = 10^{-3} S_{si}(-\frac{45.917}{T} + 0.930) , \qquad -2.06 \geq T \geq -8.2 \ ^{\circ}C \tag{3.21}$$

$$v_b = 10^{-3} S_{si}(-\frac{43.795}{T} + 1.189) , \qquad -8.2 \geq T \geq -22.9 \ ^{\circ}C \tag{3.22}$$

where v_b is volume fraction of liquid brine in saline ice and S_{si} is the Salinity of sea-ice mixture.

The real and imaginary parts of the complex dielectric constant of saline ice can be computed by the following expressions -

$$\varepsilon'_{si} = \frac{\varepsilon'_i}{1 - 3 \ v_b} , \ and \tag{2.23}$$

$$\varepsilon''_{si} = v_b \ \varepsilon''_b . \tag{3.24}$$

In the above equations, i, si and b refer to ice (pure), saline ice and brine.

3.3.3 Dielectric Constant of Snow

Snow can be divided into two categories :

(a) dry snow, which is a mixture of ice and air and contains no free water, and

(b) wet-snow, which does contain free water.

3.3.3.1 Dry Snow

The complex dielectric constant of dry snow has been calculated by using the Polder-Van Santen (1946) mixing formula for spherical inclusions with air as host dielectric and ice crystals as inclusions and is given by

$$\varepsilon'_{ds} = (1 + 0.508 \, \rho_s)^3 \; , \text{ and} \tag{3.25}$$

$$\varepsilon''_{ds} = 3 \, v_i \, \varepsilon''_i \frac{\varepsilon'_{ds}(\, 2 \, \varepsilon'_{ds} + 1 \,)}{(\varepsilon'_i + 2 \, (\varepsilon'_{ds})^2)} \tag{3.26}$$

where ρ_s is the snow density (gm/cm^3), ε'_i and ε''_i are the real and imaginary parts of the dielectric constant of pure ice and v_i is volume fraction of ice ($= \rho_s$ / 0.916). The subscripts ds and i refer to dry snow and ice respectively.

The real and imaginary parts of the dielectric constant of dry snow have been calculated using equations (3.25) and (3.26) in the frequency range of 1-37 GHz for varying snow density and surface temperature, which is used in the microwave response study of snow covered terrains.

The variation of real and imaginary parts of complex dielectric constant with snow density for varying frequencies is shown in Figure 3.2. The surface temperature is taken to be -1 $^\circ$C. The real part, i.e., dielectric permittivity (ε'_{ds}) shows almost linear increase with the increase of snow density and is independent of frequency. The value of real part of dielectric constant increases from 1.2 at snow density of 0.1 gm/cm^3 to 3.1 when snow density is 0.9 gm/cm^3. The imaginary part of dielectric constant, i.e., dielectric loss factor increases with the
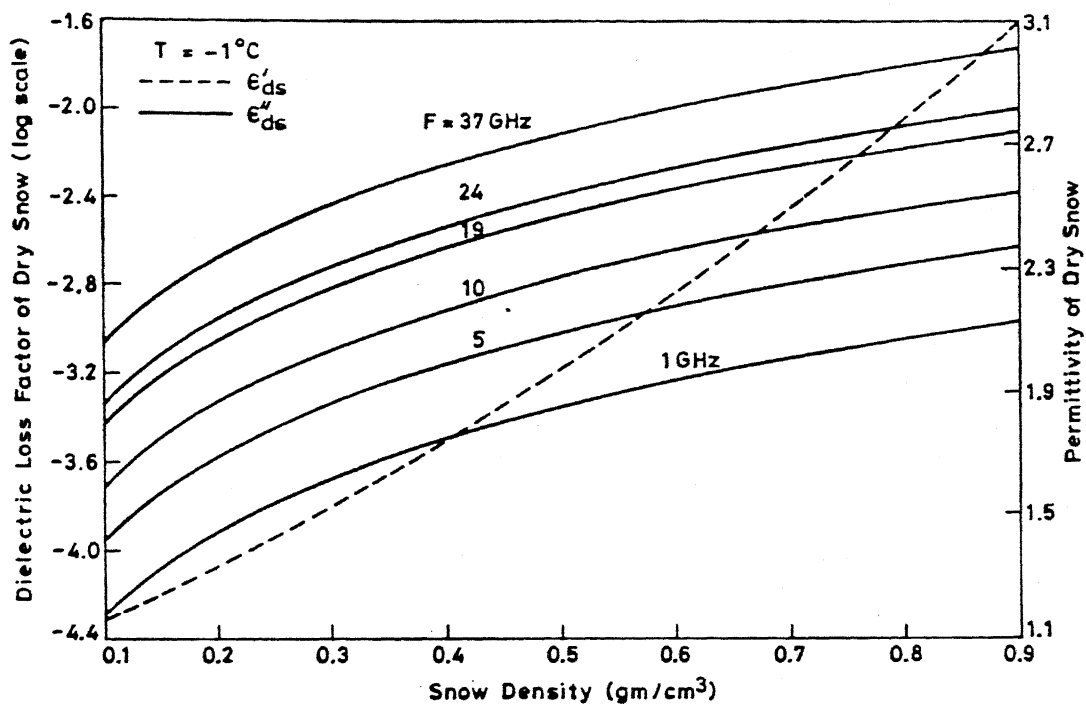
Fig. 3.2. Variation of real and imaginary parts of complex dielectric constant of dry snow (ε'_{ds} and ε''_{ds} respectively) with with snow density.

increase in frequency.

Figure 3.3 shows the variation of imaginary part of dielectric constant with frequency for varying snow density. The rate of increase of dielectric loss factor becomes higher with the increase of snow density.

The variation of loss tangent ($\tan \delta_s$) with snow density for varying surface temperature is shown in Figure 3.4. It is obvious from the figure that the loss tangent of dry snow increases with snow density as well as temperature. The variation of loss tangent for different temperatures is smaller at lower snow density and becomes significant at higher snow density.

In summary, the real part of dielectric constant of dry snow depends only upon snow density, whereas the imaginary part of dielectric constant is highly dependent on snow density, frequency, and surface temperature. The snow density is directly related to the age of the snowpack, therefore, the dielectric constant (both real and imaginary parts) of dry snow increases as ageing process prolongs.

3.3.3.2 Wet Snow

Modified Debye-like model has been used to calculate the real and imaginary parts of the dielectric constant of wet snow and is given by (Hallikainen et al., 1986)

$$\varepsilon'_{ws} = A + \frac{B \, m_v^x}{1 + (f / f_0)^2} \quad , \text{ and} \qquad (3.27)$$

$$\varepsilon''_{ws} = \frac{c \, (f / f_0) \, m_v^x}{1 + (f / f_0)^2} , \qquad (3.28)$$

34
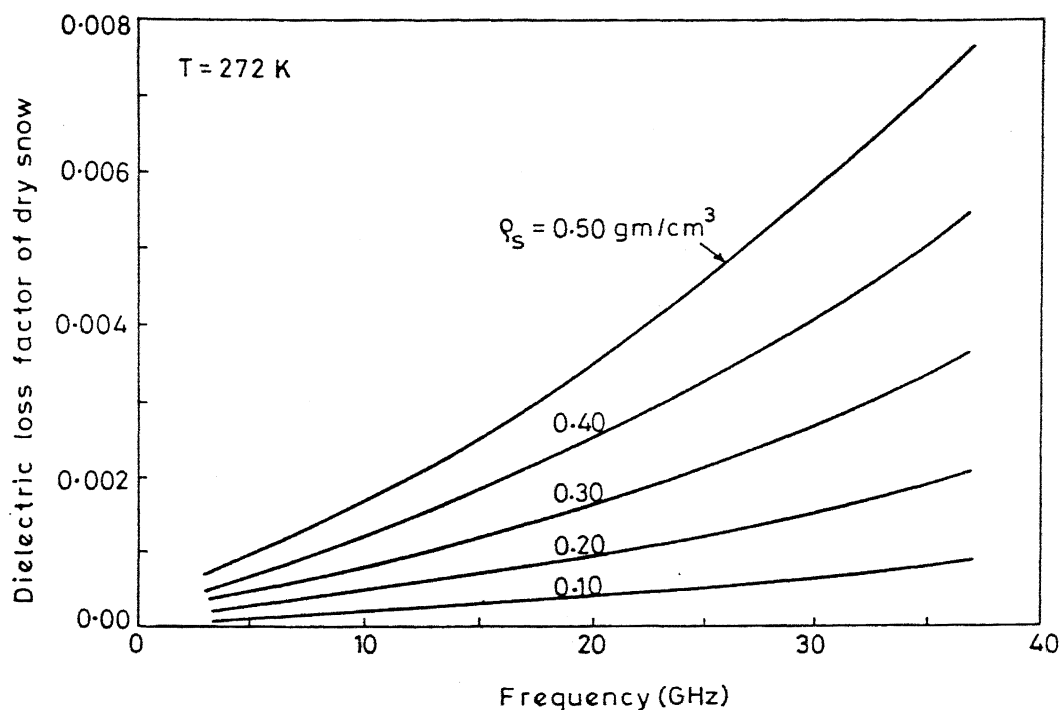
Fig. 3.3. Variation of imaginary part of dielectric constant of dry snow (ε''_{ds}) with frequency.
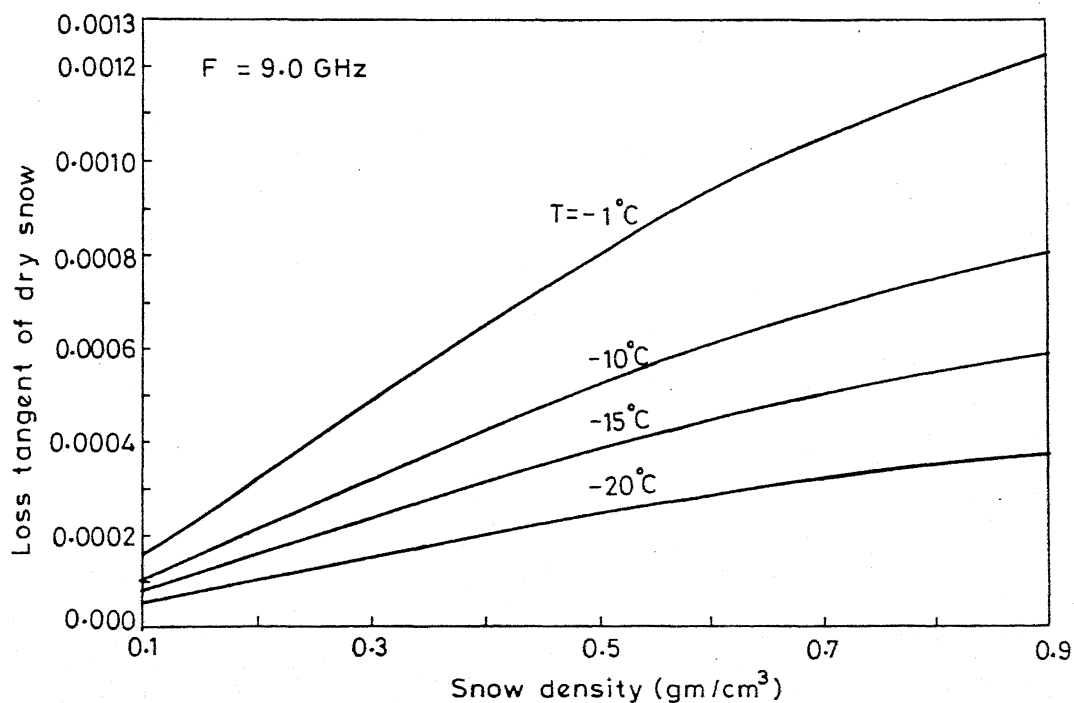
Fig. 3.4 Variation of loss tangent of dry snow (tan δ_{ds}) as a function of snow density with temperature as a parameter.

where f_0 is the relaxation frequency and m_v is liquid water content
of wet snow. The constants A, B, C, f_0 and x are determined by
the following empirical relations -

$$A = 1.0 + 1.83 \rho_s + 0.02 A_1 m_v^{1.015} + B_1 , \qquad (3.29)$$

$$B = 0.073 A_1 , \qquad (3.30)$$

$$C = 0.073 A_2 , \qquad (3.31)$$

$$x = 1.31 , \qquad (3.32)$$

$$f_0 = 9.07 \text{ GHz} , \qquad (3.33)$$

$$A_1 = 0.78 + 0.03 f - 0.58 \times 10^{-3} f^2 , \qquad (3.34)$$

$$A_2 = 0.97 - 0.39 f \times 10^{-2} + 0.39 \times 10^{-3} f^2 , \qquad (3.35)$$

$$B_1 = 0.31 - 0.05 f + 0.87 \times 10^{-3} f^2 , \qquad (3.36)$$

where f is the frequency (in GHz) of the signal used, ρ_s is the
snow density (gm/cm^3). The above expressions are valid for ranges
$3 \leq f \leq 37$ GHz, $0.09 \leq \rho_s \leq 0.38$ gm/cm^3, and $1 \leq m_v \leq 12\%$. The
subscript ws refers to wet snow.

The real and imaginary parts of the dielectric
constant of wet snow have been computed and used in all numerical
calculations by using above relations for various liquid water
content, snow density and frequency.

The behaviour of real and imaginary parts of
dielectric constant of wet snow (ε'_{ws} and ε''_{ws} respectively) with
frequency is shown in Figure 3.5 for various liquid water content
in the frequency range of 3-37 GHz. The density of wet snow is
taken to be 0.25 gm/cm^3. The real part of dielectric constant (or
dielectric permittivity) shows a decreasing trend with the increase
in frequency up to 25 GHz, and afterwards attains a constant value.
It also increases with the increase in liquid water content of snow
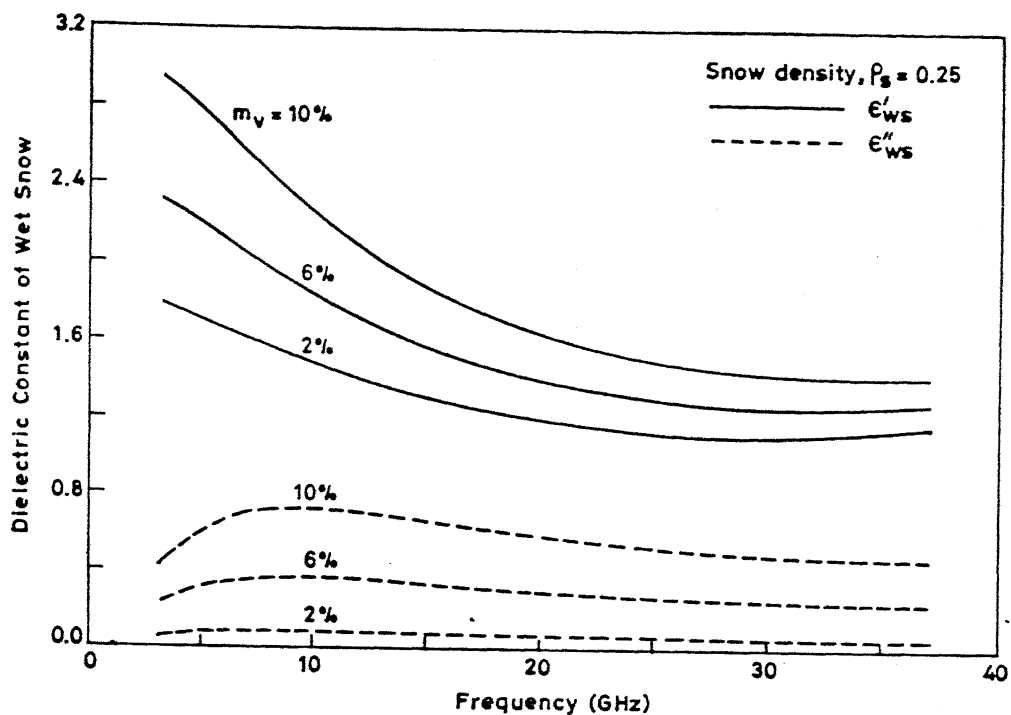
Fig. 3.5 Variation of real and imaginary parts of dielectric constant of wet snow (ε'_{ws} and ε''_{ws} respectively) with frequency for various liquid water content.
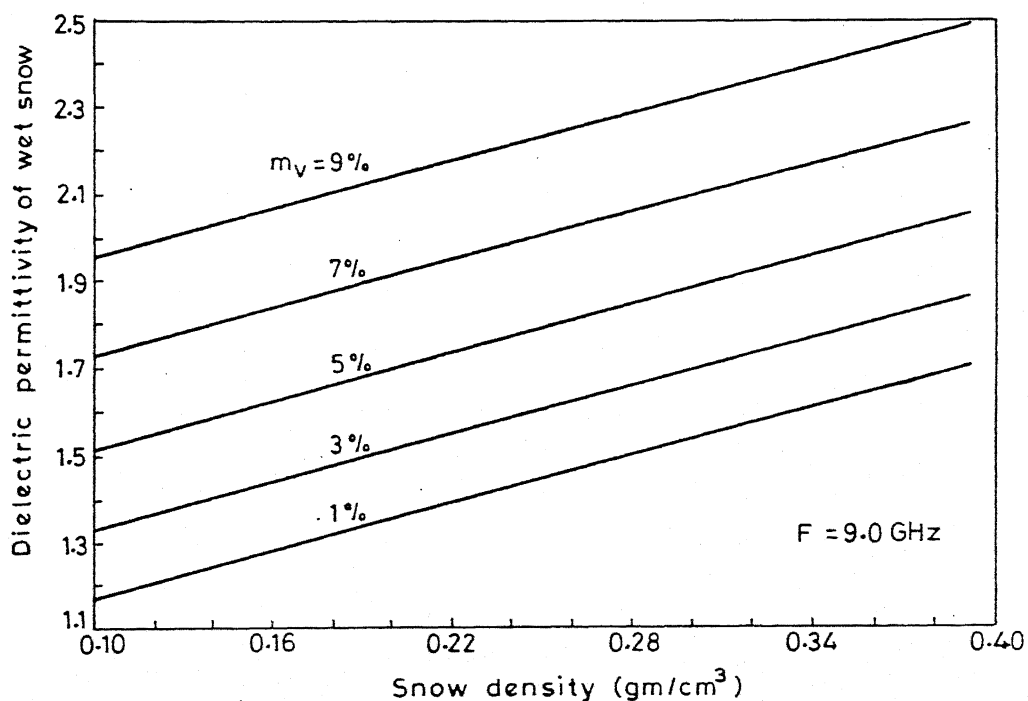
Fig. 3.6. Variation of real part of dielectric constant of wet snow as a function of snow density.

and this increase is higher at lower frequencies. The imaginary part of dielectric constant (or dielectric loss factor) first increases up to about 9 GHz and decreases thereafter continuously with the increase in frequency. The rate of increase of imaginary part of dielectric constant increases with the increase in liquid water content of snow. The values of real part of dielectric constant of wet snow at 3 GHz for 2% and 10% liquid water content are 1.8 and 2.26, and at 37 GHz for the same liquid water content are 1.16 and 1.43 respectively. The values of imaginary part of dielectric constant of wet snow at 3 GHz for for 2% and 10% liquid water content are 0.05 and 0.43, and at 37 GHz for the same liquid water content are 0.06 and 0.47 respectively.

In Figure 3.6, the variation of real part of dielectric constant of wet snow with snow density is shown at 9 GHz and for different liquid water content. The real part of dielectric constant increases linearly with the increase in density and liquid water content of snow. The dielectric permittivity of wet snow varies from 1.18 to 2.7 as the density of snow changes from 0.10 to 0.39 gm/cm^3.

The real and imaginary parts of dielectric constants of wet snow are highly dependent upon density of snow, liquid water content, and frequency. Moreover, liquid water content of snow is indirectly related to the surface temperature, therefore, the real and imaginary parts of the dielectric constant increase with the increase in surface temperature.

3.3.4 Dielectric Constant of Pure Water

The real and imaginary parts of dielectric constant of pure water has been calculated by using the well known Debye

equation (Ulaby et al., 1986) and is expressed as -

$$\varepsilon'_w = \frac{\varepsilon_{w0} - \varepsilon_{w\infty}}{1 + (2\pi f \tau_w)^2} , \qquad (3.37)$$

$$\varepsilon''_w = \frac{2\pi f \tau_w (\varepsilon_{w0} - \varepsilon_{w\infty})}{1 + (2\pi f \tau_w)^2} , \qquad (3.38)$$

where

ε_{w0} = static dielectric constant of pure water,

$\varepsilon_{w\infty}$ = high-frequency limit of ε_w (= 4.9),

τ_w = relaxation time of pure water, and

f = electromagnetic frequency.

The static dielectric constant of pure water (ε_{w0}) and the relaxation time of pure water (τ_w), are functions of water temperature and are given by

$$2\pi\tau_w (T) = 1.1109 \times 10^{-10} - 3.824 \times 10^{-12} T + 6.938$$
$$\times 10^{-14} T^2 - 5.096 \times 10^{-16} T^3 , \qquad (3.39)$$

$$\varepsilon_{w0}(T) = 88.045 - 0.4147 T + 6.295 \times 10^{-4} T^2$$
$$+ 1.075 \times 10^{-5} T^3 , \qquad (3.40)$$

where T is in ^oC. The subscript w refers to pure water.

3.3.5 Dielectric Constant of Saline Water

Saline water is a water containing dissolved salts. The real and imaginary parts of the dielectric constant of saline water can be expressed as-

39

$$\varepsilon'_{sw} = \varepsilon_{sw\infty} + \frac{\varepsilon_{sw0} - \varepsilon_{sw\infty}}{1 + (2\pi f \tau_{sw})^2} \quad , \text{ and} \qquad (3.41)$$

$$\varepsilon''_{sw} = \frac{2\pi f \tau_{sw} (\varepsilon_{sw0} - \varepsilon_{sw\infty})}{1 + (2\pi f \tau_{sw})^2} + \frac{\sigma_i}{2\pi \varepsilon_0 f} \quad , \qquad (3.42)$$

where the subscript sw refers to saline water, σ_i is the ionic conductivity of the aqueous saline solution and $\varepsilon_{sw\infty} = \varepsilon_{w\infty} = 4.9$. The dependence of static dielectric constant (ε_{w0}) on water salinity S_{sw} (‰) and surface temperature ($T^{o}C$) is given by

$$\varepsilon_{sw0}(T,S_{sw}) = \varepsilon_{sw0}(T,0) \cdot a(T,S_{sw}) \quad , \qquad (3.43)$$

where

$$\varepsilon_{sw0}(T,0) = 87.134 - 1.949 \times 10^{-1} T - 1.276 \times 10^{-2} T^2$$
$$+ 2.491 \times 10^{-4} T^3 \quad , \qquad (3.44)$$

and

$$a(T,S_{sw}) = 1.0 + 1.613 \times 10^{-5} T S_{sw} - 3.656 \times 10^{-3} S_{sw}$$
$$+ 3.210 \times 10^{-5} S^2 - 4.232 \times 10^{-7} S^3 \quad . \qquad (3.45)$$

The relaxation time is given by

$$\tau_{sw}(T,S_{sw}) = \tau_{sw}(T,0) \cdot b(T,S_{sw}) \quad , \qquad (3.46)$$

where $\tau_{sw}(T,0) = \tau_w(T)$ (see eqn. 3.39), and

$$b(T,S_{sw}) = 1.0 + 2.282 \times 10^{-5} T S_{sw} - 7.638 \times 10^{-4} S_{sw}$$
$$- 7.76 \times 10^{-6} S^2_{sw} + 1.105 \times 10^{-8} S^3_{sw} \quad . \qquad (3.47)$$

The ionic conductivity for saline water (σ_i) given by Stogryn (1971) takes the form

$$\sigma_i(T, S_{sw}) = \sigma_i(25, S_{sw}) \, e^{-\phi} , \tag{3.48}$$

where $\sigma_i(25, S_{sw})$ is the ionic conductivity of sea water at 25 °C and is given by

$$\sigma_i(25, S_{sw}) = S_{sw} [0.18252 - 1.4619 \times 10^{-3} S_{sw} - 2.093$$
$$\times 10^{-5} S_{sw}^2 - 1.282 \times 10^{-7} S_{sw}^3] . \tag{3.49}$$

The function ϕ depends on S_{sw} and $\Delta = 25 - T$,

$$\phi = [2.033 \times 10^{-2} + 1.266 \times 10^{-4} \Delta + 2.464$$
$$\times 10^{-6} \Delta^2 - S_{sw} (1.849 \times 10^{-5} - 2.551$$
$$\times 10^{-7} \Delta + 2.551 \times 10^{-8} \Delta^2)] \tag{3.50}$$

The combination of all the above equations are valid for the salinity range of 4 to 35 %. .

3.3.6 Dielectric constant of bare ground

The dielectric constant of bare ground (ε_g) has been computed by using a semi-empirical model (Dobson et al., 1985), which is given by

$$\varepsilon_g^\alpha = 1 + \frac{\rho_b}{\rho_{ss}} (\varepsilon_{ss}^\alpha - 1) + m_v^\beta (\varepsilon_w^\alpha - 1) , \tag{3.51}$$

where ρ_b is the bulk soil density (gm/cm^3), ρ_{ss} is the density of solid soil material (= 2.65 gm/cm^3), ε_{ss} is the complex dielectric constant of solid soil material (= 4.7 - j 0), m_v is the liquid water content of soil, and ε_w is the complex dielectric constant of water. The values of α and β are taken to be 0.65 and 1.0 (optimum for all soil types).

CHAPTER 4

RESULTS AND DISCUSSIONS

4.1 INTRODUCTION

In order to study the potentiality of microwave radiometers on board and to aid the analysis and interpretation of microwave remote sensing data, the knowledge of snow and ground parameters affecting the microwave remote sensing response is very much essential. In the present work, the theoretical response of microwave remote sensing over snow covered terrains is studied. The study has been carried out over various two-layered and multi-layered models representative of snow covered terrains. The results of the detailed numerical calculations are presented to study the potentiality of passive microwave radiometry to retrieve snowpack parameters, to map the snow cover, to monitor snowmelt, to estimate the thickness of natural lake ice, and to suggest the optimum sensor parameters to be used in the polar and mid- to high-lattitude regions. The variation of model parameters of snow as well as the penetration depth of microwaves in the snow medium with varying physical parameters in the frequency range of 1-37 GHz are also studied. In all the calculations, the real part of relative dielectric constant of pure ice is taken 3.15 (as mentioned in chapter 3) and imaginary part is taken from Figure 3.1. The real and imaginary parts of dielectric constants of dry and wet snow are taken as discussed in sections 3.3.3.1 and 3.3.3.2.

4.2 MODEL PARAMETERS OF SNOW

The model parameters of snow, i.e., scattering (k_s), absorption (k_a), and extinction (k_e) coefficients govern the emission behaviour of the snowpack. The snow particles have been taken as spherical and uniformly distributed. The model parameters have been computed by utilizing Rayleigh expressions for given physical properties of the snow medium like snow density, radius of snow particles, liquid water content etc.

Using equations (2.8) to (2.24), we have studied the propagation characteristics of snow. The results are shown in Figures 4.1-4.3. Figure 4.1 demonstrates the variation of scattering (k_s), absorption (k_a), and extinction $(k_e=k_a+k_s)$ coefficients of dry snow with frequency for snow particles of 1.0 mm size. It is evident from the Figure 4.1 that the loss of electromagnetic energy due to absorption is more than the loss due to scattering up to 19 GHz, and afterwards scattering becomes the dominant loss mechanism. The behaviour of model parameters of dry snow with the snow particles radius for 10 and 19 GHz is shown in Figure 4.2. It is clear from the Figure 4.2 that the scattering, absorption and extinction losses are more for 19 GHz than that at 10 GHz. It can be seen that the absortion coefficient is independent of the snow particles size, whereas scattering coefficient is highly dependent on snow particles size. For smaller particles, absorption plays an important role, whereas for larger particles, scattering becomes the primary loss process.

The variation of absorption, scattering, and extinction coefficients of wet snow with the radius of snow particles is shown in Figure 4.3 for 10 and 19 GHz frequency.
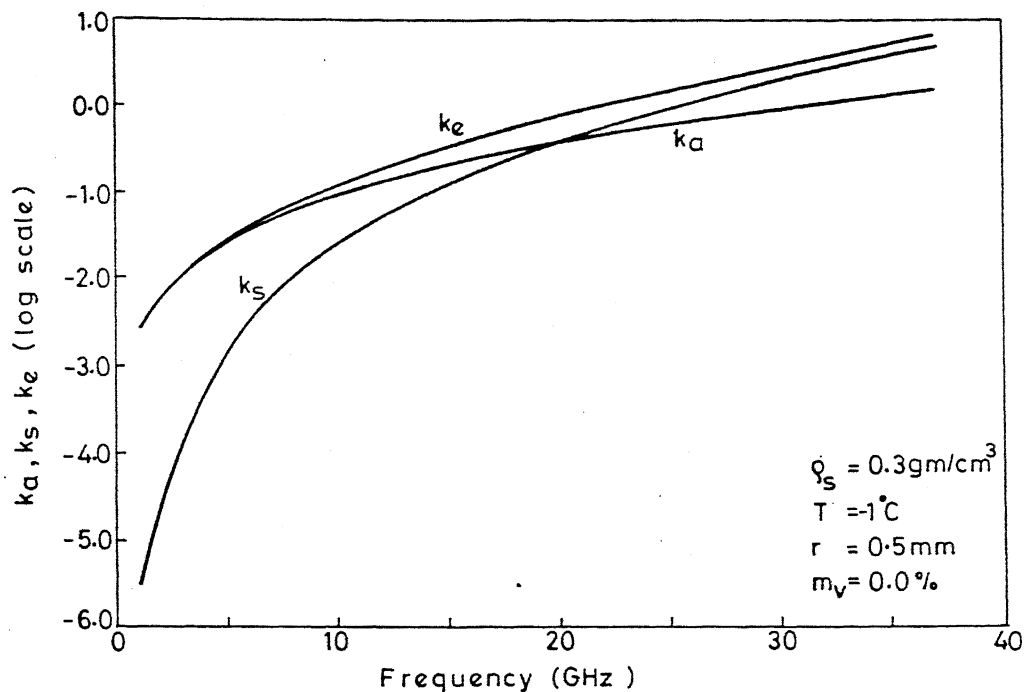
Fig. 4.1. Spectral variation of scattering (k_g), absorption (k_a) and extinction coefficients (k_e) of dry snow.

Fig. 4.2. Variation of scattering (k_g), absorption (k_a) and extinction (k_e) coefficients of dry snow with the radius of snow particles.

The liquid water content of snow is taken 1.0% . The behaviour of scattering and absorption coefficients is same as shown in Figure 4.2. It is clear from Figure 4.3 that the absorption loss dominates over scattering loss in the presence of even a small amount of liquid water.

The absorption and scattering losses are highly dependent on microwave frequencies, and particles size and liquid water content of snow. At low frequencies, when the size of snow particles is much smaller than wavelength, absorption plays an important role, whereas at higher frequencies when the size of the snow particles is of the order of wavelength, scattering becomes significant. The absorption is the primary loss process in wet snow. Moreover, The total loss of electromagnetic energy is much higher for wet snow as compared to that of dry snow.

4.3 PENETRATION DEPTH OF MICROWAVES IN SNOW MEDIUM

The penetration depth of microwaves in the snow medium is the function of the frequency of microwave signal, and particles size and liquid water content of snow. In Figure 4.4, the variation of penetration depth with density of dry snow (m_v =0.0%) for various snow particle sizes is shown at 19 GHz. The penetration depth of microwave signal initially decreases rapidly with the increase in snow density and attains a constant depth value, which is an optimum penetration depth. The penetration depths of microwave signal (F=19 GHz) in dry snow of density 0.1 gm/cm^3 and snow particles of radius 0.5, 1.0, 1.5 and 2.0 mm are 28.0, 21.0, 12.3, and 7.0 meters respectively.

The penetration depth of microwave signal (F=19 GHz)
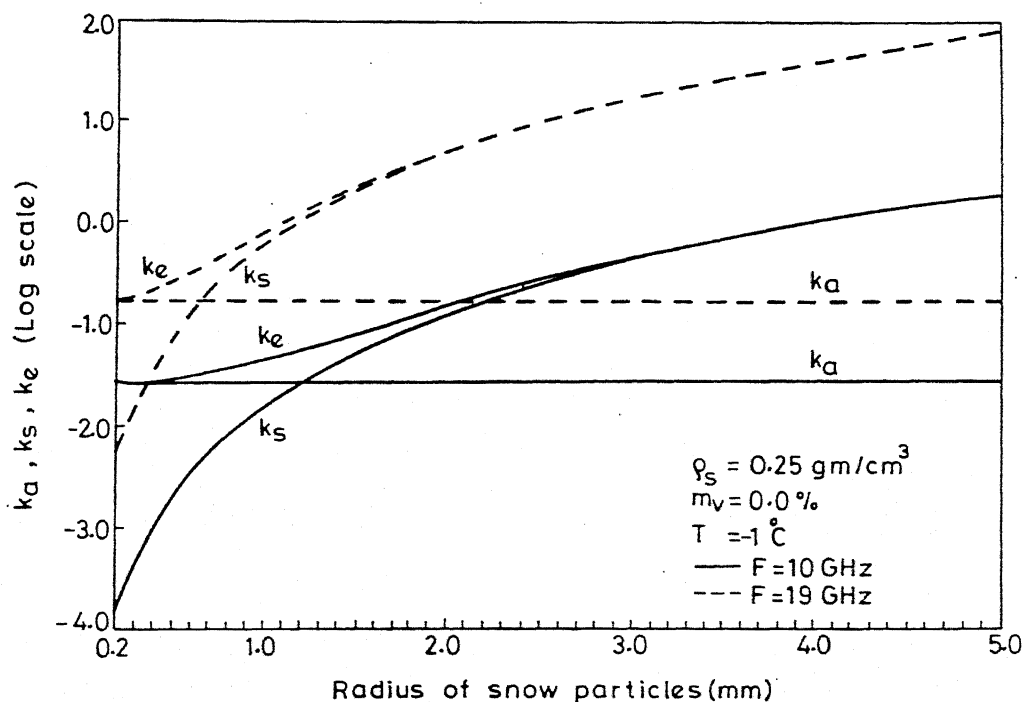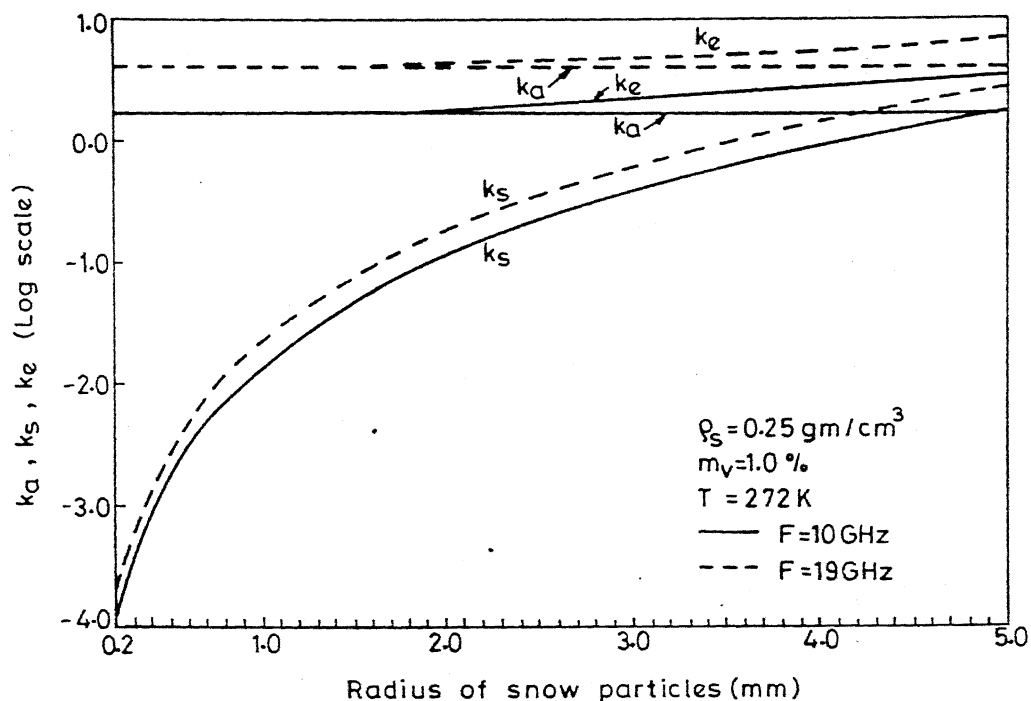
Fig. 4.3. Variation of scattering (k_s), absorption (k_a) and extinction (k_e) coefficients of wet snow with the radius of snow particles.
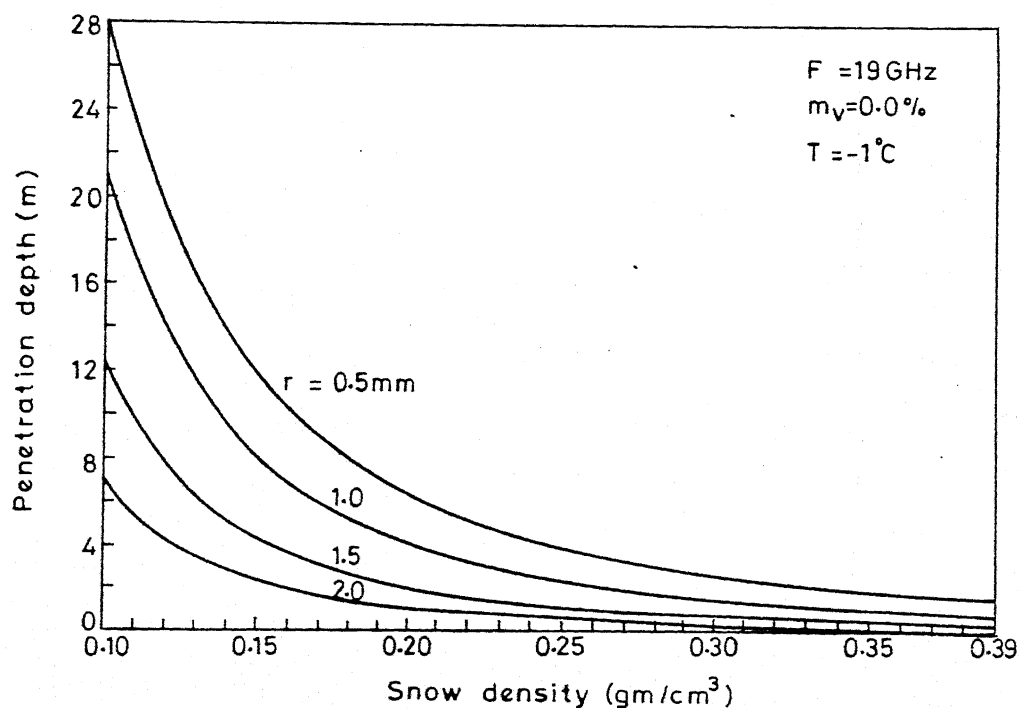
Fig. 4.4. Variation in penetration depth of microwave signal as a function of dry snow density.

with wet snow density is shown in Figure 4.5. The penetration depth is strongly reduced when the snow is wet. The decrease in penetration depth is because of the fact that total loss of electromagnetic energy due to scattering and absorption is very high in case of wet snow as compared to that of dry snow. Here, it can be seen that penetration depth remains same for different particle sizes up to snow density of 0.19 gm/cm^3. The penetration depth of microwave signal at 19 GHz in wet snow is approximately 48 cm for snow density of 0.10 gm/cm^3.

Figure 4.6 shows the variation of penetration depth in wet snow (density = 0.25 gm/cm^3, and radius of snow particles = 0.5 mm) with moisture content for varying frequencies. Because of the increase in dielectric constant of snow with moisture content and consequently total loss of electromagnetic energy, penetration depth reduces continuously with the increase in liquid water content of snow. The penetration depth also decreases as the frequency of microwave signal increases.

4.4 PASSIVE MICROWAVE REMOTE SENSING RESPONSE OF SNOW COVERED TERRAINS

Snow covered terrains can be represented as two-layered and multi-layered models. The physical and electromagnetic properties of each snow layer and underlying ground control the microwave remote sensing response. As discussed in Chapter 2, in passive microwave remote sensing, brightness temperature is measured from which snow layer characteristics are deduced. The detailed study of brightness temperature behaviour has been carried out over various two-layered and multi-layered models
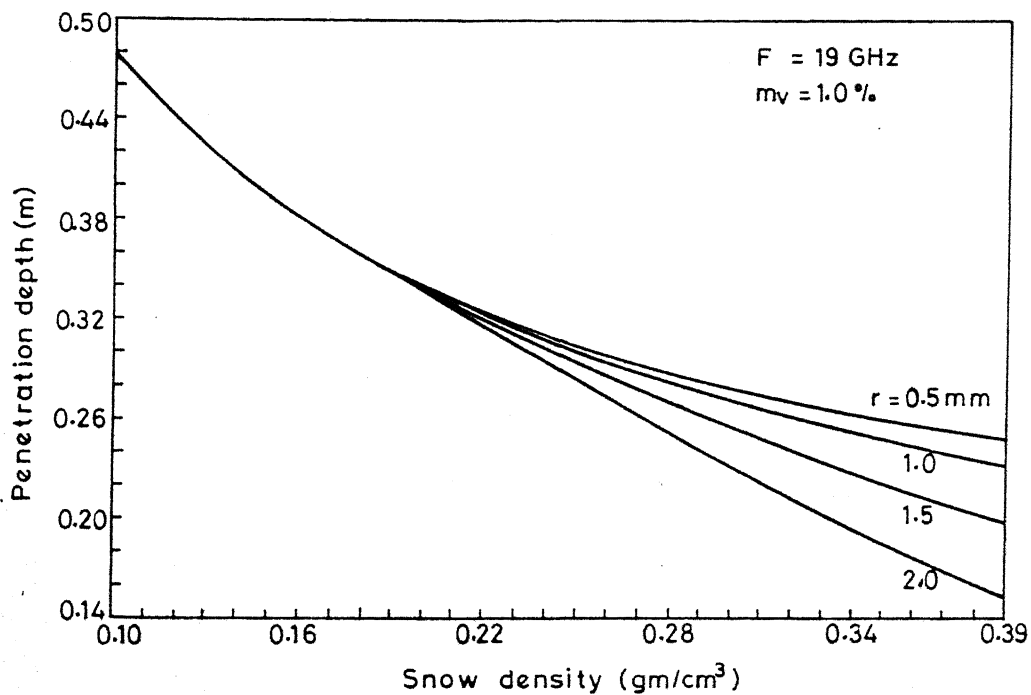
Fig. 4.5. Penetration depth of microwave signal versus wet snow density.
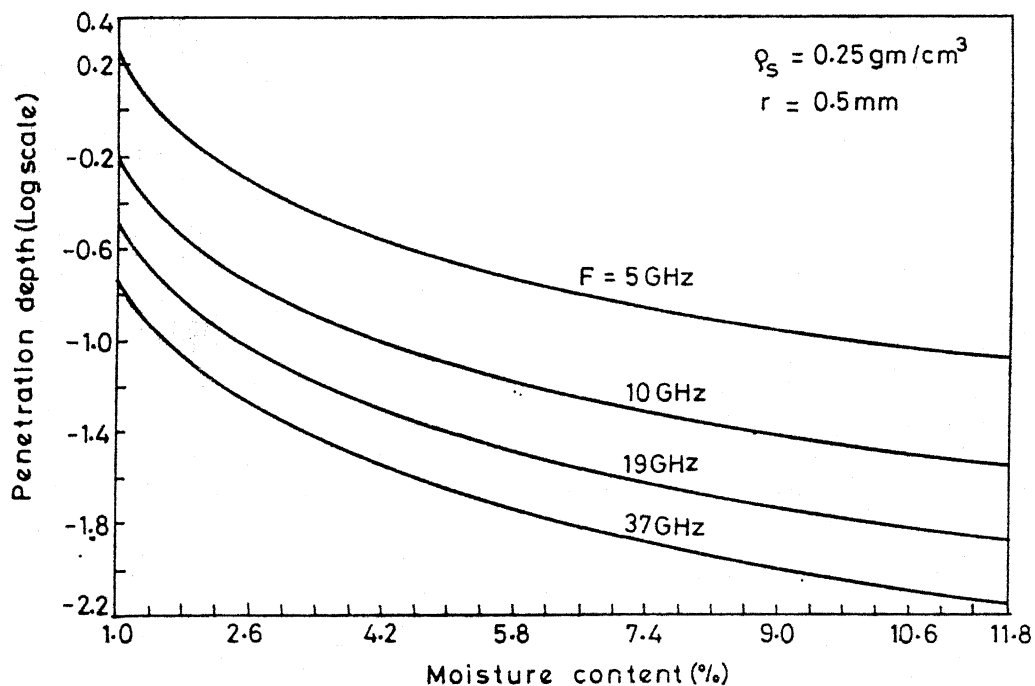
Fig. 4.6. Variation in penetration depth of microwave signal with liquid water content of snow.

representative of snow covered terrains in mid- to high-lattitude and mountaineous regions.

4.4.1 Two - Layer Models

A snow covered region can be represented as a simple two-layered model. In order to study the difference in microwave remote sensing response over bare ground and snow covered ground, brightness temperature has been computed with various sensor and layered (snow) parameters. In Figure 4.7, frequency response of brightness temperature in vertical and horizontal polarizations for microwave signals incident at 30° is shown for bare ground and ground covered with dry and wet snow. The density and average snow particles size are 0.25 gm/cm^3 and 1.6 mm respectively. The brightness temperature of ground covered with dry snow shows decresing trend with the increase in frequency. For snow-free and wet snow covered ground, brightness temperature shows increasing trend. The brightness temperature contrast in vertical and horizontal polarizations is significant at lower frequencies and becomes negligible at higher frequencies for wet snow. Moreover, at higher frequencies, contrast between the brightness temperature of dry snow and wet snow and that of dry snow and bare ground is very pronounced. However, it is difficult to separate the areas covered with wet snow from snow-free areas in both the polarizations.

The extinction loss of dry snow is very small up to about 19 GHz and microwaves are capable to penetrate through the snow layer. Therefore, at low frequencies, brightness temperature behaviour is mainly determined by the underlying ground
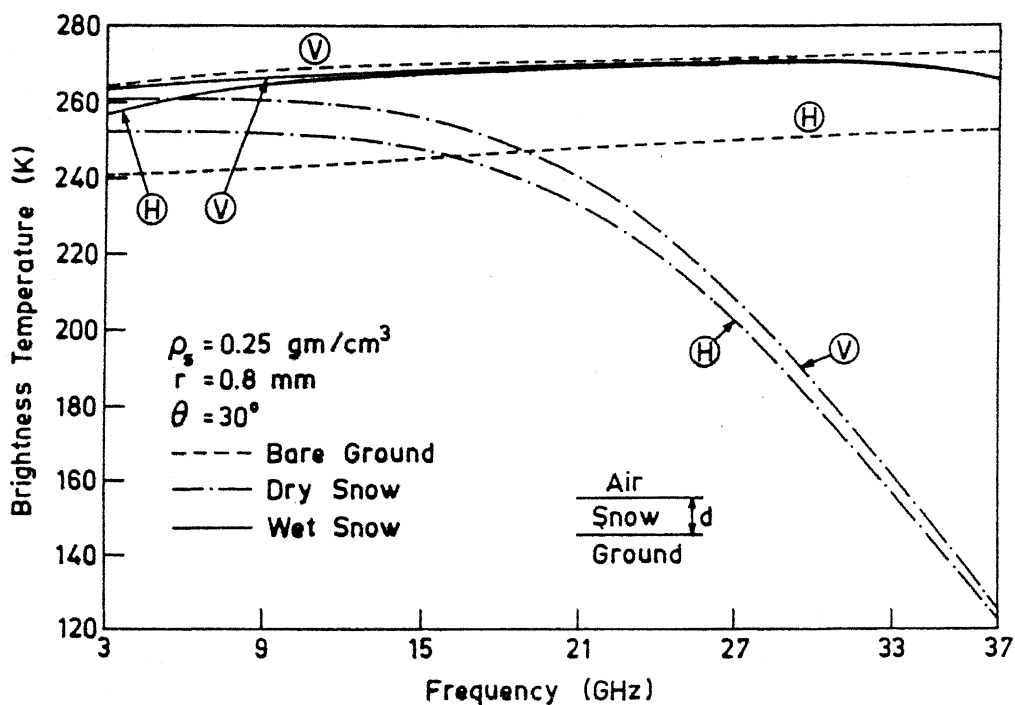
Fig. 4.7. Frequency response of brightness temperature of snow covered and bare ground (m_v of dry snow = 0.0%, m_v of wet snow = 1.0%, m_v of bare ground = 5%, temperature of dry snowpack = 272.0 $^\circ$K, temperature of wet snowpack = 275.0 $^\circ$K, temperature of bare ground = 298.0 $^\circ$K, bulk soil density = 1.7 gm/cm^3).

and at higher frequencies by the snow layer. However, in the case of wet snow, brightness temperature behaviour is mainly governed by the snow layer. Therefore, a sudden decrease in brightness temperature is encountered when going from bare ground and ground covered with wet snow to the ground covered with dry snow in the frequency range of 19-37 GHz.

The brightness temperature contrast in two polarizations ($T_{BV} - T_{BH}$) with frequency is shown in Figure 4.8 for the same models. The brightness temperature contrast ($T_{BV} - T_{BH}$) for dry snow is almost frequency independent up to 15 GHz and afterwards it shows a decreasing trend. For wet snow, it shows a decreasing trend up to 27 GHz before attaining a constant value, whereas it decreases slowly in the case of bare ground for the entire frequency range. The brightness temperature contrast ($T_{BV} - T_{BH}$) is very small for wet snow as compared to that of bare ground.

Figure 4.9 demonstrates the angular dependence of brightness temperature at 19 GHz of bare ground and ground covered with dry and wet snow for the models discussed earlier. The brightness temperature decreases in horizontal polarization and increases in vertical polarization as the incidence angle increases. For bare ground, the brightness temperature in horizontal as well as in vertical polarization is highly dependent on incidence angle; and for wet snow, the brightness temperature contrast in both the polarizations is insignificant even at very high incidence angle. Therefore, to discriminate the snow-free areas from areas covered with wet snow, incidence angle of 50° may prove to be ideal.

The negative spectral behaviour of brightness
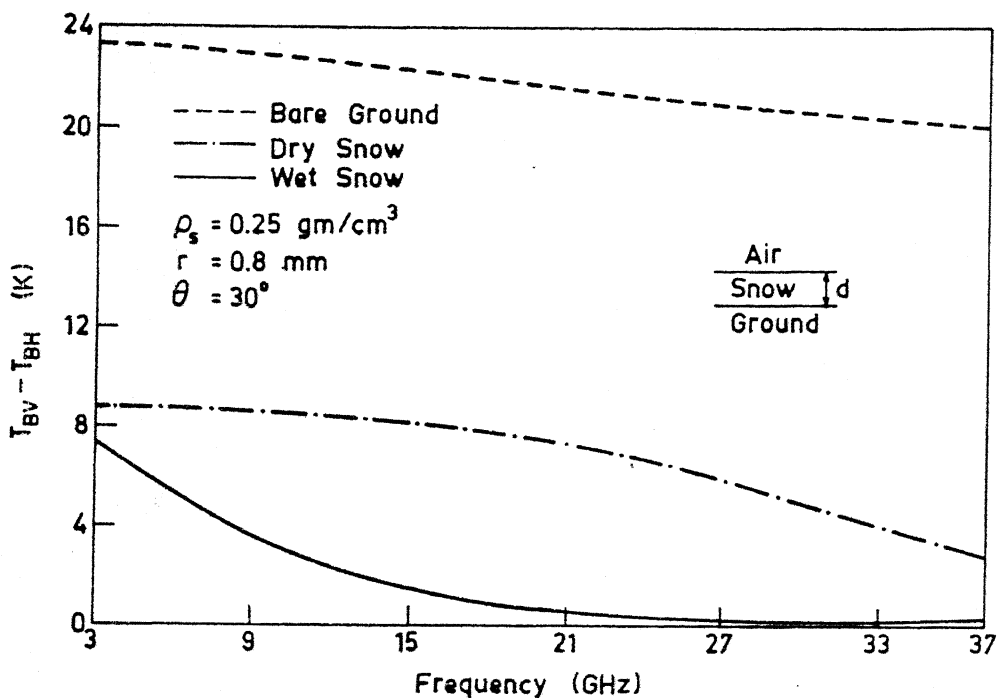
Fig. 4.8. Variation of brightness temperature contrast in vertical and horizontal polarizations ($T_{BV} - T_{BH}$) with frequency.
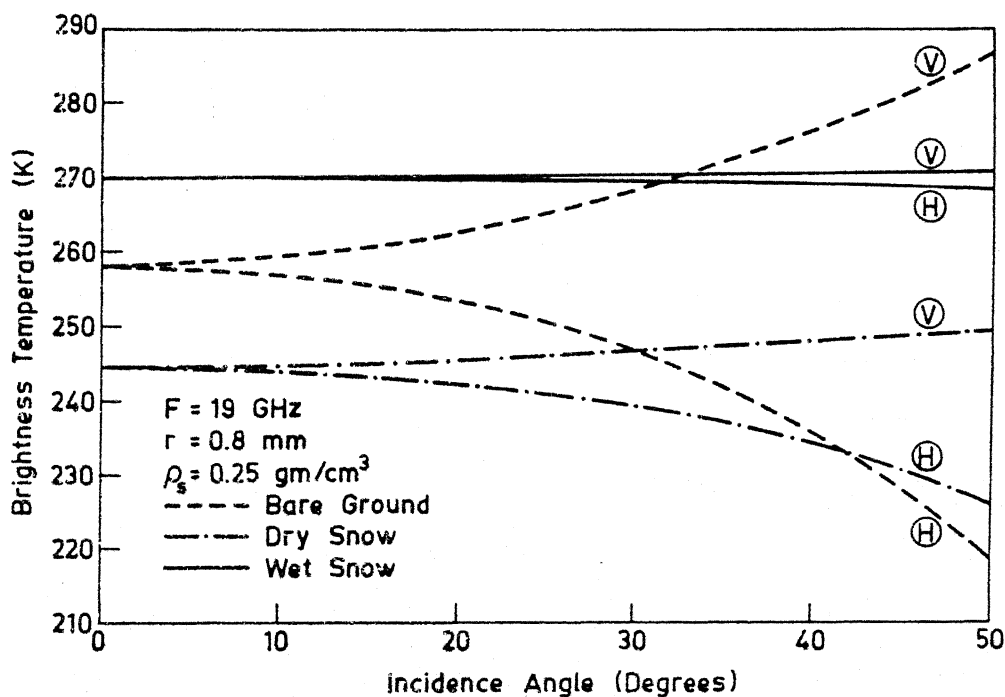
Fig. 4.9. Angular dependence of brightness temperature for snow covered and bare ground.

temperature in dry snow is the unique property for distinguishing it from wet snow and bare ground. The polarization information may improve the separability between the bare ground and ground covered with wet snow. Hence, mapping of snow cover as well as classification of snow types, i.e., the discrimination of dry and wet snow is possible on the basis of brightness temperature behaviour shown in the broad band frequencies.

Snowpack usually undergoes several melting and refreezing cycles, as a result, the size of snow particles gets changed throughout its life history. The size of snow particles increases significantly with slight wetting. In Figure 4.10, the frequency response of brightness temperature for varying snow particle sizes and snow layer thicknesses is shown at 50° look angle and horizontal polarization. The brightness temperature remains constant up to about 9 GHz for snow particles of 0.8 and 1.2 mm radii, and decreases sharply thereafter before attaining a constant value. As shown in Figure 4.10, the brightness temperature decreases as the particle size and depth of snow layer increase. For very small particles, brightness temperature is less sensitive to snow thickness.

The brightness temperature behaviour with snow particles size is shown in Figure 4.11 for 15, 19, 25 and 37 GHz and at look angle of 50°. As discused in the section 4.2, scattering losses dominate a dry snow cover as the frequency and snow particles size increase, which causes the reduction in brightness temperature. The decreasing trend of brightness temperature increaes with the increase of frequency. For the snow layers containing particles of 0.2 and 2.0 mm radii, the brightness
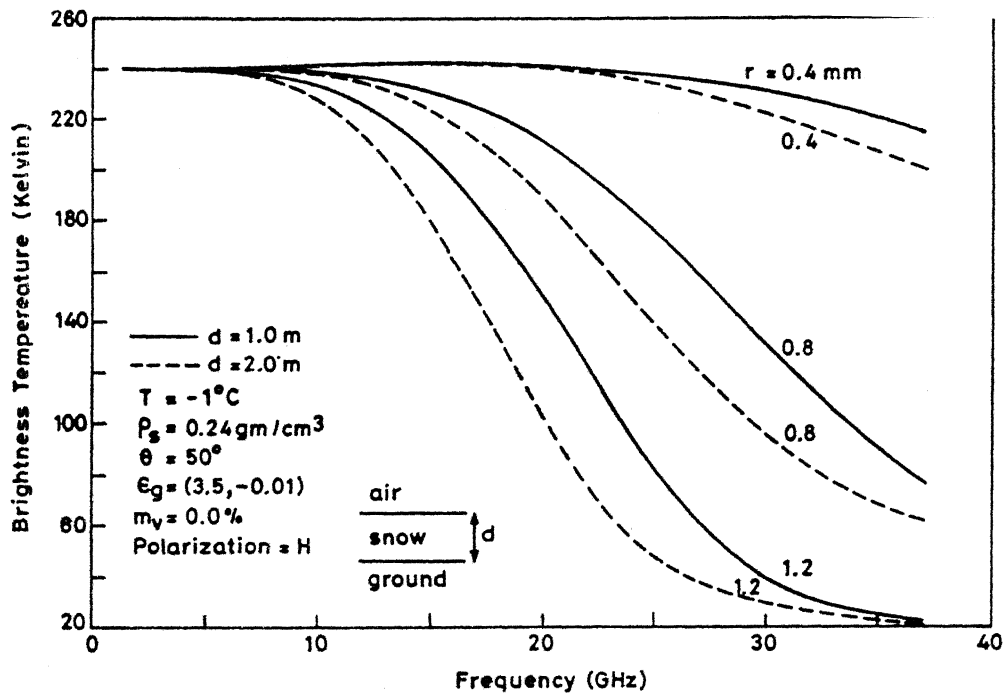
Fig. 4.10. Frequency response of brightness temperature of two-layered model for varying snow particle sizes and snow thicknesses.
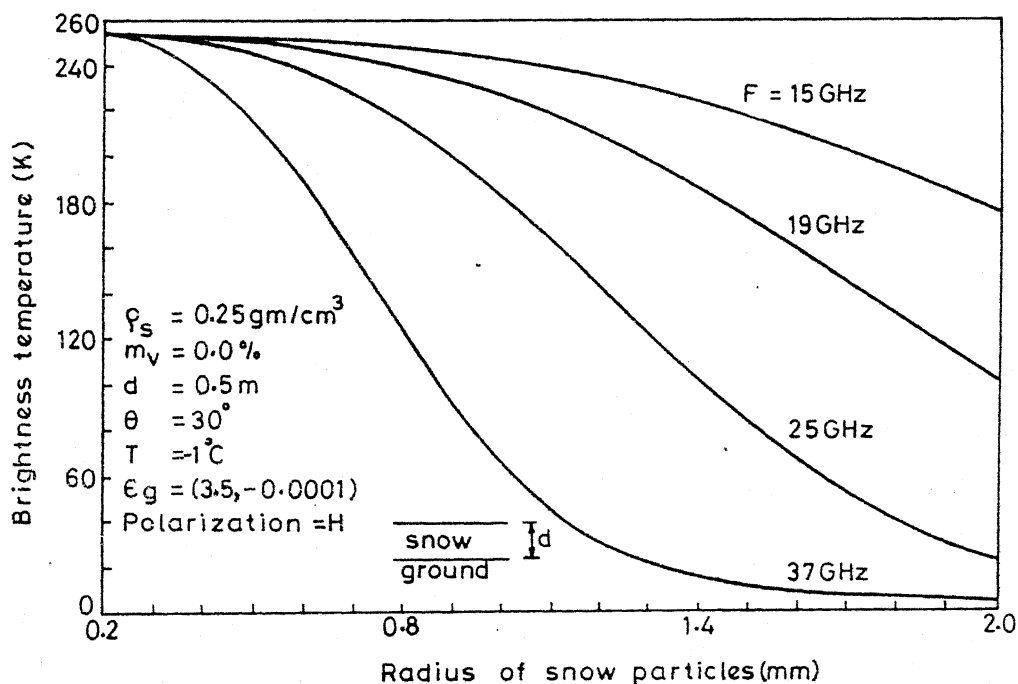
Fig. 4.11. Variation of brightness temperature as a function of radius of snow particles for varying frequencies.

temperatures are approximately 254.0 and 180.0°K respectively at 15 GHz and are 254.0 and 5.0 $^{\circ}$K respectively at 37 GHz. From Figure 4.11, it is concluded that for very small snow particles, the brightness temperature is independent of frequency, whereas for larger particles it shows very strong frequency dependence.

To estimate the daily snow cover extent and accurate runoff from a snow covered area, knowledge of snow thickness is very important (Schultz, 1988). Figure 4.12 shows the behaviour of brightness temperature with snow thickness for 19, 25, and 37 GHz and look angles of 30° and 50°. The average snow particles size is taken 1.0 mm. At 19 GHz, brightness temperature is almost independent of the thickness of the snow layer and as the frequency increases, the negative slope of the curve increases. The brightness temperature decreases as the look angle increases from 30° to 50°. However, the behaviour of brightness temeprature is similar for 30° and 50° look angles. It is evident from the Figure that for snow layer containing particles of 1 mm size, more accurate estimation of snow thickness can be made at 37 GHz.

The effect of snow particles size and thickness on brightness temperature at 37 GHz and 30° look angle is shown in Figure 4.13. The brightness temperature first decreases with the increase in snow thickness and becomes constant after a saturation depth for a particular size of snow particles. For larger snow particles, scattering loss of electromagnetic energy becomes so significant that even a small increase in the thickness of snow layer results in a drastic decrease in brightness temperature. Therefore, thickness of snow containing larger particles can not be inferred at 37 GHz. For snow particles of 1.0 mm size, the
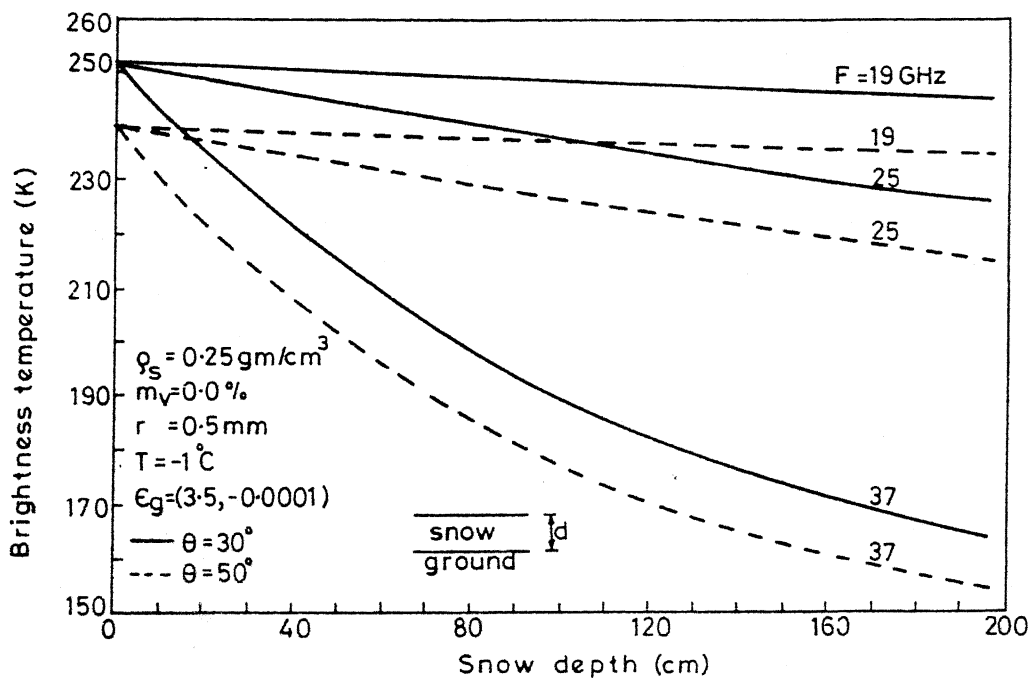
Fig. 4.12. Variation of brightness temperature with snow thickness for varying frequencies and look angles.
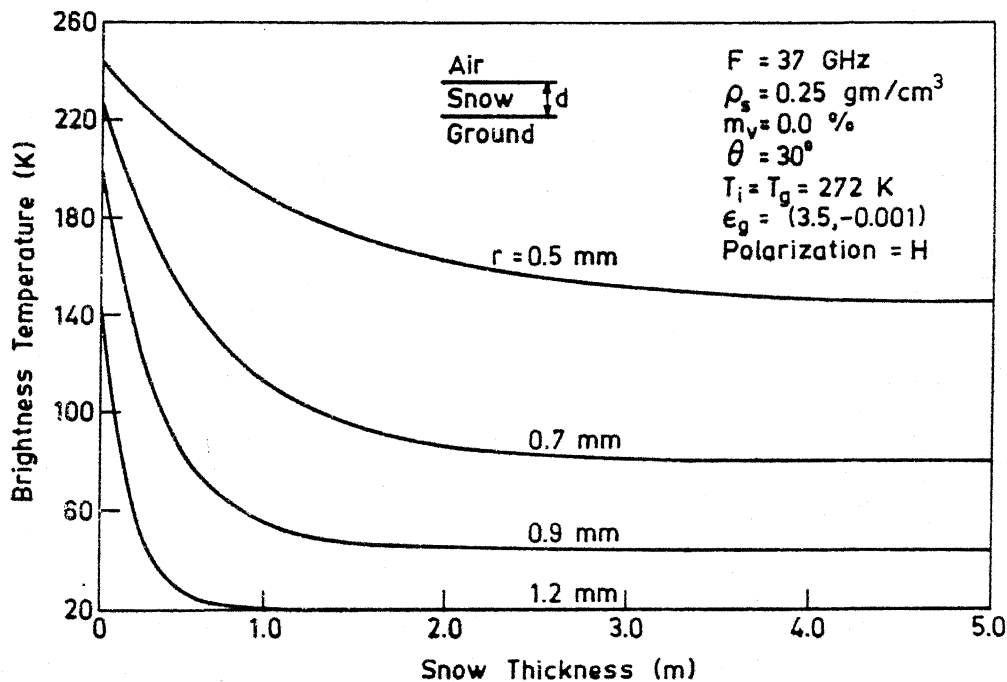
Fig. 4.13. Variation of brightness temperature as a function of snow thickness with snow particle size as a parameter.

snow layer thickness upto about 2.5 m can be estimated accurately.

Therefore, the thickness of snow layer and particle size strongly influence the emission behaviour of the snowpack. The determination of snow water equivalent, i.e., how much water can be derived from a snow covered area $(= \int_0^d \rho_s \, dz$, where d is the thickness of the snow layer) is very important for the prediction of runoff from a river basin. The penetration depth of microwaves in wet snow is very small (as discussed in section 4.3), therefore, the thickness of wet snow can not be estimated. The size of snow particles generally varies between 1 to 2 mm. Therefore, for average size of snow particles, frequency range of 25-37 GHz will be suitable for the extraction of snow thickness information.

The snow wetness parameter is very important in estimating water reserve for irrigation and hydropower (Schultz, 1988). The variation of brightness temperature as a function of frequency for various snow water content is shown in Figure 4.14 in horizontal and vertical polarizations. For vertical polarization, brightness temperature remains nearly constant up to approximately 30 GHz and is followed by a slight decrease. In case of horizontal polarization, the brightness temperature increases sharply up to 27 GHz and decreases thereafter. The decrease in brightness temperature may be attributed to the dominating behaviour of scattering as loss mechanism at higher frequencies. The variation in brightness temperature due to the change in liquid water content of snow is hardly discernable in vertical polarization. Therefore, vertical polarization is not at all suited for the estimation of
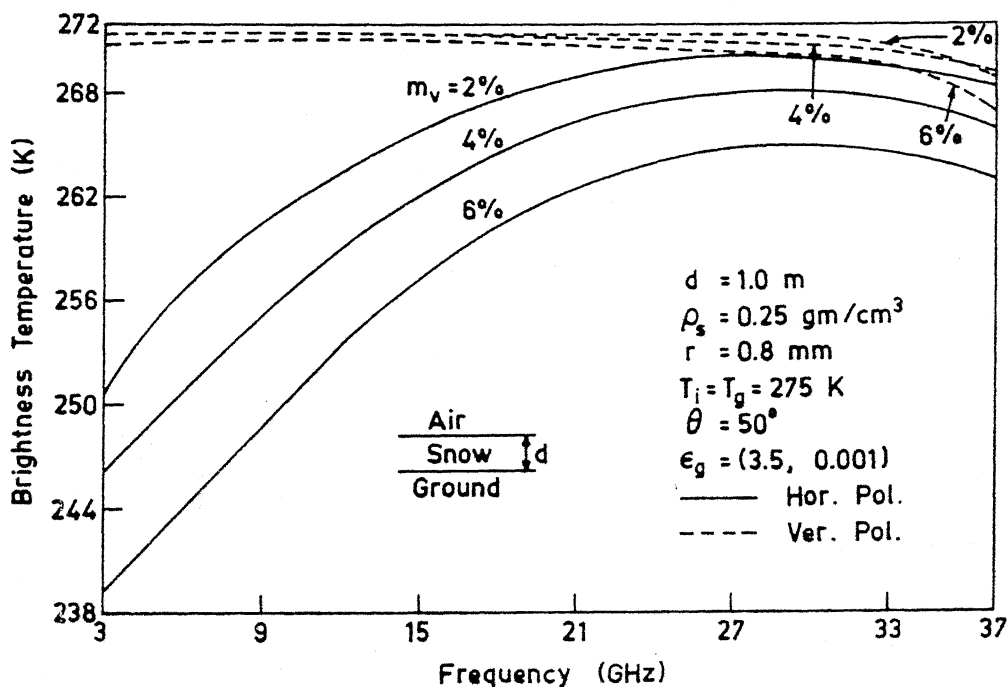
Fig. 4.14. Frequency response of brightness temperature of wet snow with liquid water content of snow as a parameter.
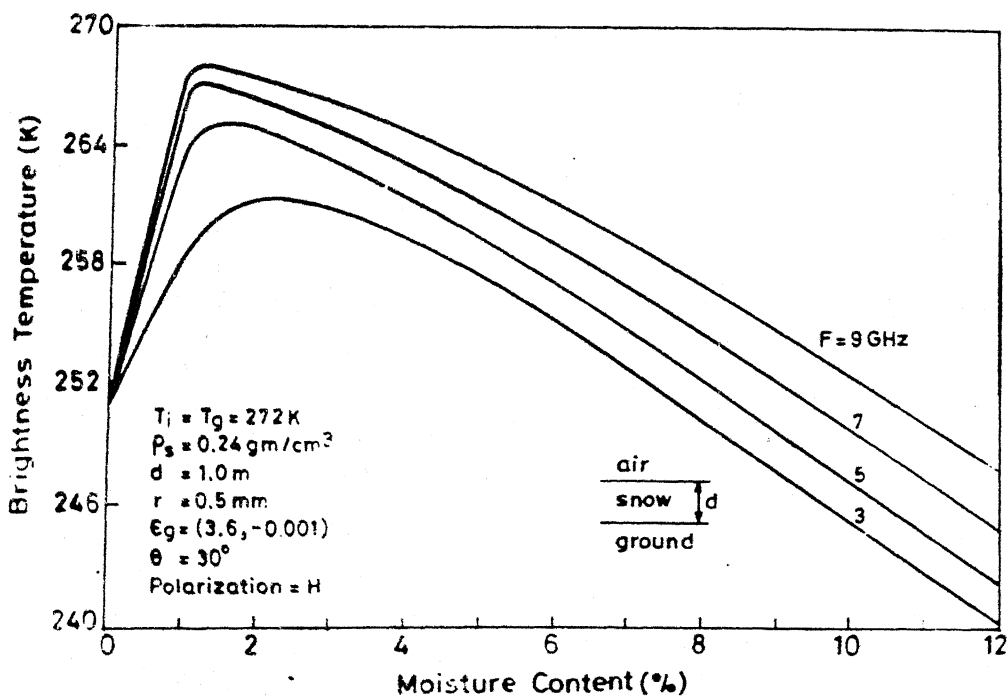
Fig. 4.15. Brightness temperature versus liquid water content of snow for different frequencies.

water content of snow. However, the brightness temperature variation for different water content is significant in horizontal polarization.

In order to estimate the free liquid water content in snow, the effect of snow water content on brightness temperature is shown in Figure 4.15 for various frequencies. The average size of the snow particles is taken to be 1.0 mm. It is obvious from the Figure that the brightness temperature of dry snow remains lower than that of wet snow up to about 8% liquid water content (except 3 GHz) and is higher for further increase in snow wetness. For 3 GHz, the brightness temperature initially increases upto 2.5% snow water content and then decreases continuously, whereas for higher frequencies brightness temperature increases only upto 1% snow water content and decreases afterwards. It is evident from the Figure 4.15 that a particular brightness temperature represents two values of snow water content. Moreover, at lower frequencies the brightness temperature of dry snow becomes higher than that of wet snow with higher liquid water content. To resolve this ambiguity, multi-frequency approach should be preferred. At higher frequency, the decreasing trend of brightness temperature with the increase in liquid water content (after 1%) decreases. Therefore, in order to estimate the liquid water content of snow precisely, lower frequencies must be used.

The information of onset of snow melt can also be made available, which is a very important parameter for the prediction of timing of runoff from a river basin. Snow becomes wet during the day time and becomes dry in the night time. This phenomenon can be used to detect the onset of snow melt because a

large diurnal fluctuation in brightness temperature will be observed at higher frequencies, especially at 37 GHz (from Figures 4.7 and 4.14).

Generally, the interfaces between air and snow medium, and snow and ground medium are seldom smooth due to the presence of snow melting and local winds. In order to study the effect of surface roughness on microwave remote sensing response, brightness temperature as a function of frequency is shown in Figure 4.16 for smooth and rough (σ = 1 cm) surfaces of dry and wet snowpacks. The average temperatures of dry and wet snowpacks are taken to be 272 and 275 $^{\circ}$K respectively. The brightness temperature is higher when the upper surface of dry snow is rough in 3-18 GHz frequency range and is lower after 18 GHz. In the case of wet snow, the variation in brightness temperature is significant at lower frequencies and is hardly discernable at higher frequencies. As shown in Figure 4.16, the surface roughness effect in case of dry snow is minimised at 18 GHz.

The angular dependence of brightness temperature at 10 GHz is shown in Figure 4.17 for the same model parameters as discussed in Figure 4.16. The variation in brightness tempearature in horizontal polarization for plane and rough surfaces increases as the incidence angle increases, whereas in the case of vertical polarization it shows just opposite behaviour to that of horizontal polarization. It is clear from the Figure 4.17 that the effect of surface roughness is almost eliminated in vertical polarization at about 50° look angle. Moreover, brightness temperature contrast ($T_{BV} - T_{BH}$) decreases as roughness is introduced.

To study the roughness effect of top and bottom
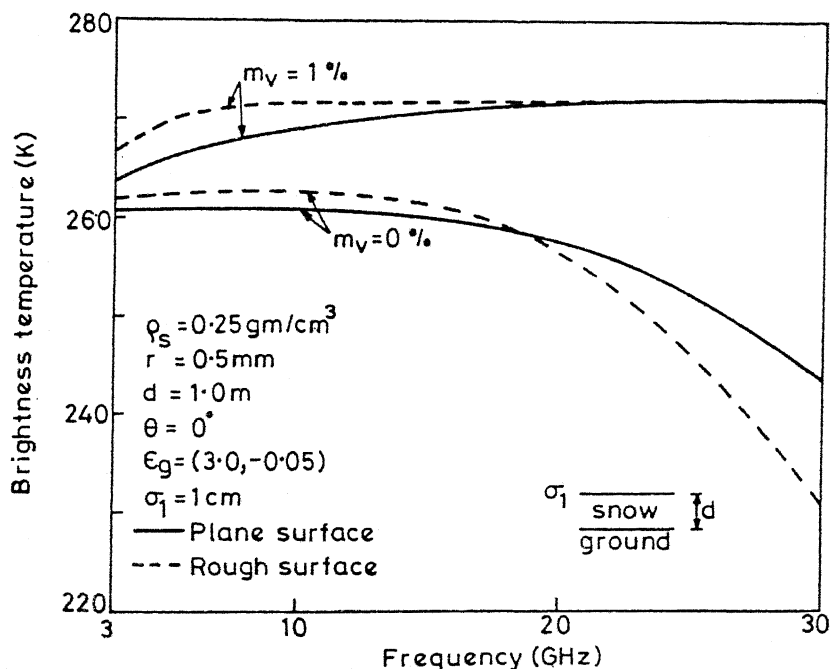
Fig. 4.16. Spectral variation of brightness temperature for smooth
and rough top snow surfaces.
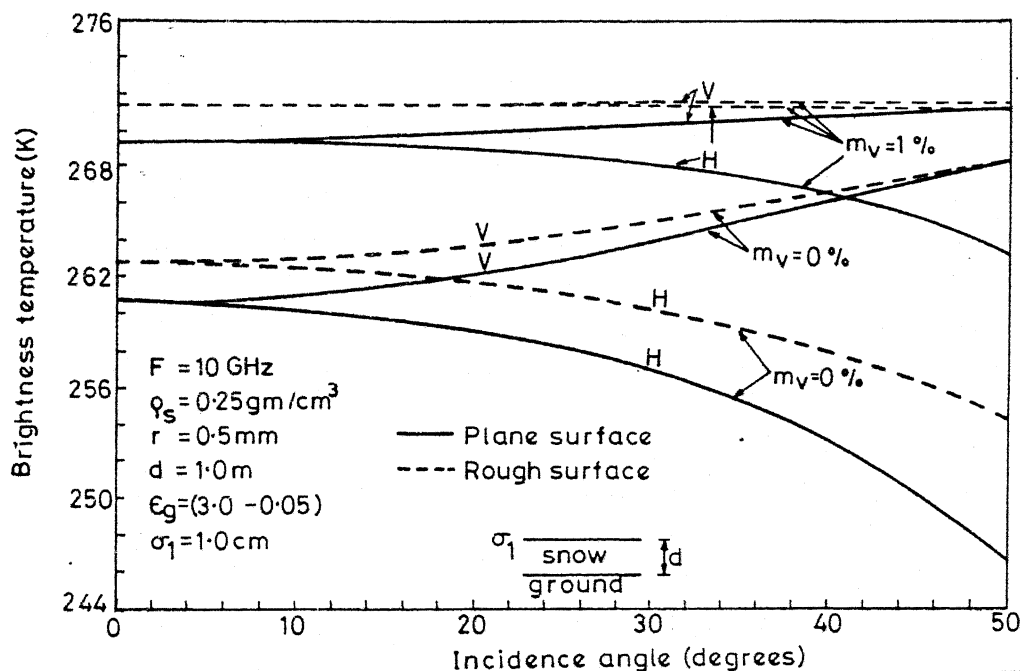
Fig. 4.17. Angular dependence of brightness temperature for smooth
and rough top snow surfaces.

surfaces of dry snowpack, angular dependence of emissivity is shown in Figure 4.18 at 5 GHz frequency. It shows that at lower frequency (i.e., when penetration depth is large) bottom surface topography plays an important role in governing the emission behaviour of the snowpacks.

4.4.2 MULTI-LAYER MODELS

Variable exchange of heat and mass on the snow surface leads to accumulation of snow in layers. The physical characteristics of these layers differ from one to another. As the thickness of snow increases, the bottom layers become more compact and dense. Due to equilibrium thermodynamics, crystals of small sizes and of spherical shape are developed and when there is a steep temperature gradient with depth, large crystals are developed. Here, the passive microwave remote sensing response of multi-layered models representative of mountaineous and polar regions is discussed for various physical conditions. In all the models, the temperatures of dry and wet snow layers are assumed to be 272.0 and 275.0^{o}K respectively.

Figure 4.19 shows the frequency response of brightness temperature in horizontal and vertical polarizations for the models given in the legend. The moisture content and thickness of each snow layer are taken to be 0.0% and 10 cm respectively. The brightness temperature in both the polarizations remains same for the two models up to 11 GHz and is higher afterwards for the model (1) in which the snow particles size decreases with depth as compared to the model (2) in which the snow particles size increases. The brightness temperature contrast between the two
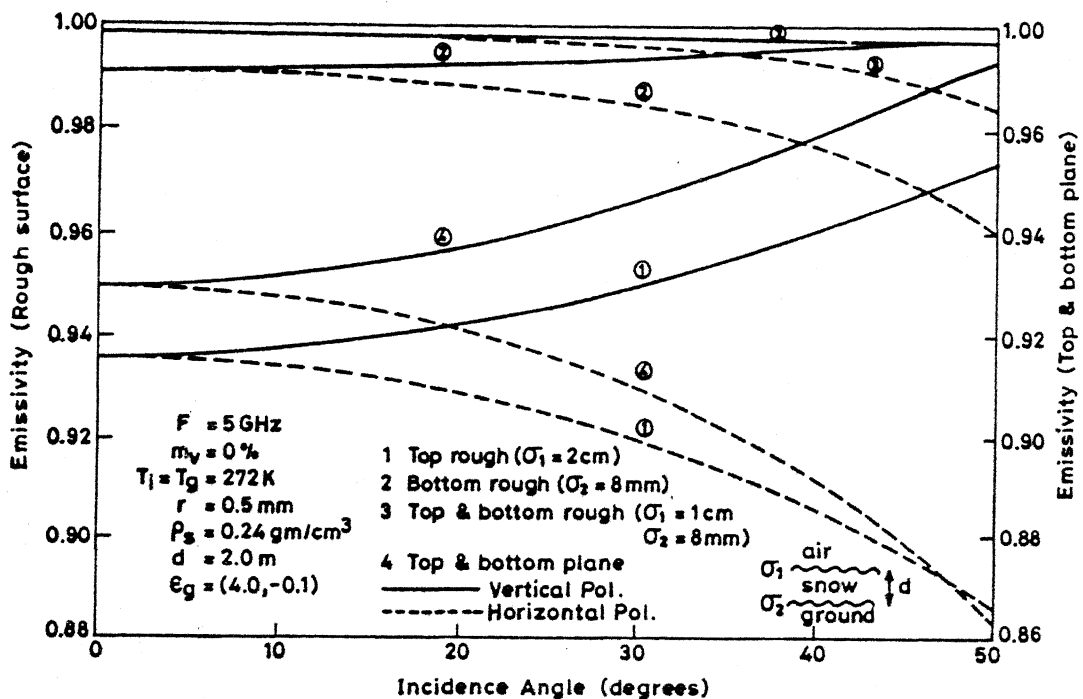
Fig. 4.18 Effect of top and bottom surface roughness of snow on emissivity.
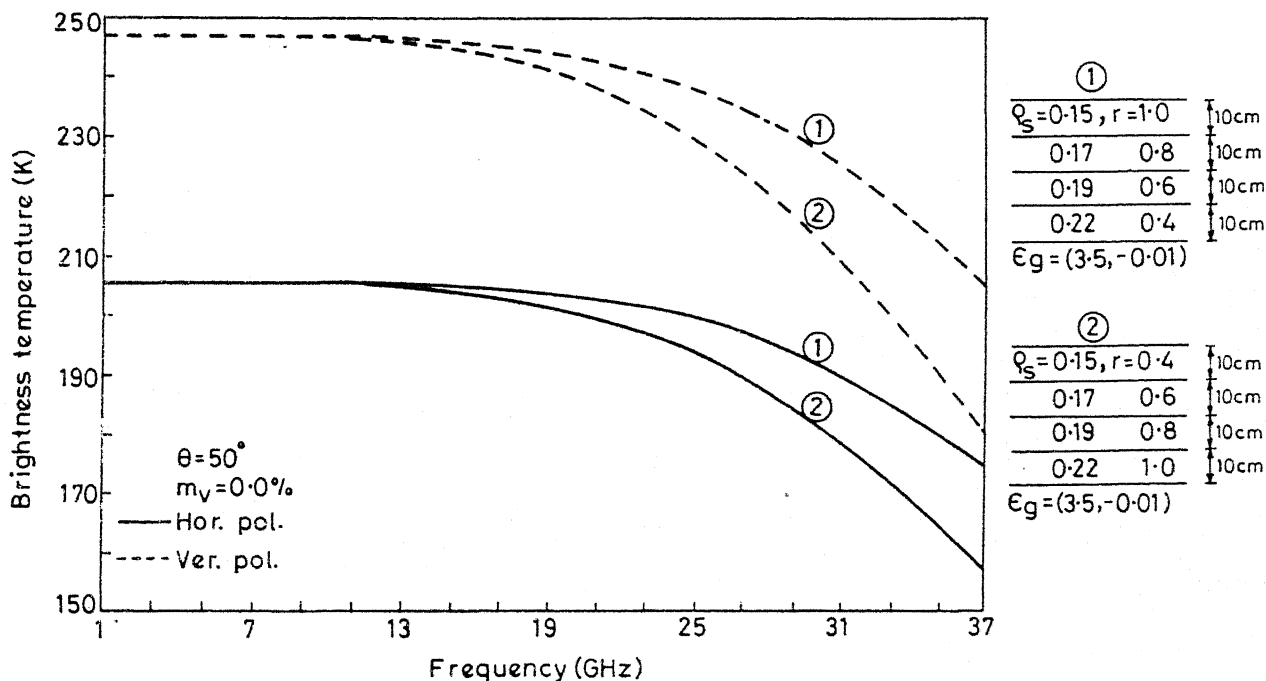
Fig. 4.19 Spectral variation of brightness temperature for multi-layered models with decreasing and increasing snow particles size with depth.

models is higher in vertical polarization than horizontal polarization.

The frequency response of brightness temperature in vertical and horizontal polarizations over models representative of yearly and multiyear snowpacks is shown in Figure 4.20. The yearly and multiyear snow layers are charactarized with varying density and particle size of snow. The moisture content and thickness of each snow layer are taken to be the 0.0% and 20 cm respectively. The behaviour of brightness temperature is similar as earlier. In horizontal polarization, as the number of layers of the snowpacks increases, the brightness temperature decreases significantly for the entire frequency range. However, in vertical polarization, the brightness temperature remains same for the models (1) and (2) up to about 13 GHz frequency and as the frequency increases, snowpacks containing lesser number of layers show higher brightness temperature. The brightness temperature contrast for the three models increases with the increase of frequency in vertical polarization.

The angular dependence of brightness temperature for the same models (as in Figure 4.20) is shown in Figure 4.21. The brightness temperature decreases with the increase of incidence angle in horizontal polarization, whereas it increases in vertical polarization. The brightness temperature contrast in both the polarizations $(T_{BV} - T_{BH})$ decreases with the decrease in the number of snow layers, i.e., multiyear snowpacks show higher brightness temperature contrast. Therefore, it can be concluded that the use of proper frequency and polarization measurements can reveal information about the age of accumulated snow.

Snow undergoes melting and refreezing cycles with time in response to change in weather conditions. There are two types of melting and refreezing cycles — (i) when the upper layers of the snowpack are wet and as the temperature falls, the whole snowpack refreezes, and (ii) when the whole snowpack is wet and the upper layer refreezes during cold nights. In order to monitor the melting and refreezing cycles, frequency response of brightness temperature in horizontal polarization is shown in Figure 4.22. The physical parameters of each snow layer are given in the legend of the Figure. In the melting and refreezing cycle of type 1, i.e., when the upper layers of the snowpack are wet, brightness temperature increases sharply up to 9 GHz and this rate decreases with further increase of frequency in horizontal polarization. But as the temperature falls and snowpack refreezes, brightness temperature first remains constant up to 15 GHz and decreases rapidly afterwards. In the case of refreezing and melting cycle of type 2, i.e., when the whole snowpack is wet, brightness temperature follows the same behaviour as the snowpack of early stage of type 1. In the later stage of the cycle of type 2, as the upper layer refreezes, brightness temperature first shows increasing trend up to 15 GHz and decreases rapidly thereafter. The brightness temperature of snowpack containing only one layer of snow with 1% liquid water content is higher (however, variation in brightness temperature is small) as compared to that of wet multi-layered snowpacks (2 and 3). In vertical polarization, almost same behaviour is observed (shown in Figure 4.23). However, in vertical polarization, brightness temperature is less sensitive to the changes that occur during the two types of melting and refreezing

Top figure legend:
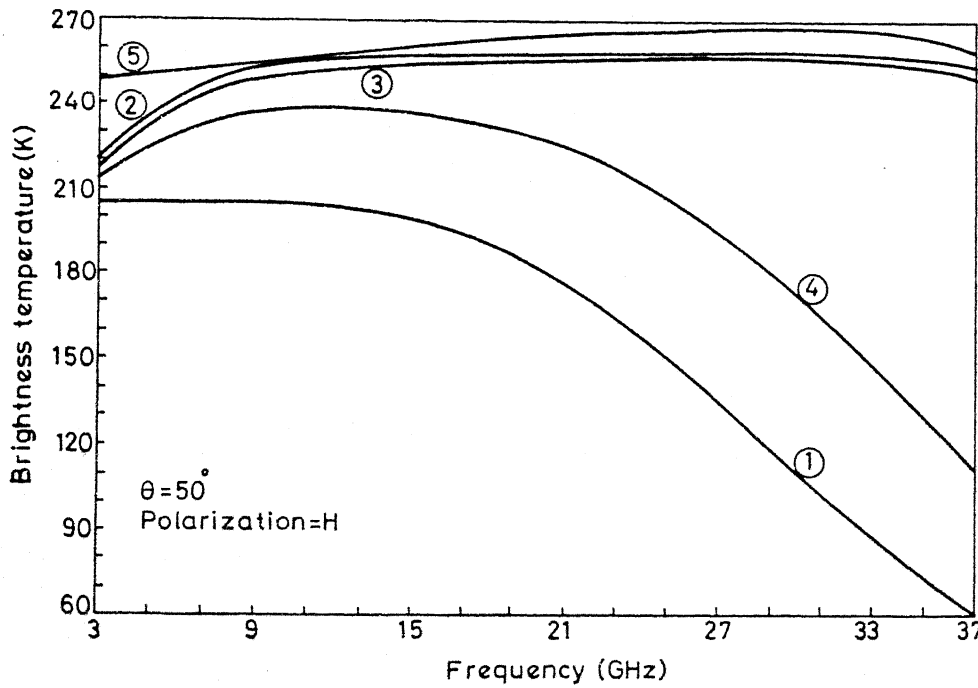
① $\rho_s = 0.25, r = 1.0, m_v = 0\%$ 20cm
   0.30, 0.8,   0% 20cm
   0.35, 0.6,   0% 20cm
   0.40, 0.4,   0% 20cm
$\epsilon_g = (3.5, -0.05)$

② $\rho_s = 0.25, r = 1.0, m_v = 2\%$ 20cm
   0.30, 0.8,   1% 20cm
   0.35, 0.6,   0% 20cm
   0.40, 0.4,   0% 20cm
$\epsilon_g = (3.5, -0.05)$

③ $\rho_s = 0.25, r = 1.0, m_v = 1\%$ 20cm
   0.30, 0.8,   1% 20cm
   0.35, 0.6,   1% 20cm
   0.40, 0.4,   1% 20cm
$\epsilon_g = (3.5, -0.05)$

④ $\rho_s = 0.25, r = 1.0, m_v = 0\%$ 20cm
   0.30, 0.8,   1% 20cm
   0.35, 0.6,   1% 20cm
   0.40, 0.4,   1% 20cm
$\epsilon_g = (3.5, -0.05)$

⑤ $\rho_s = 0.25, r = 1.0, m_v = 1\%$ 20cm
$\epsilon_g = (3.5, -0.05)$
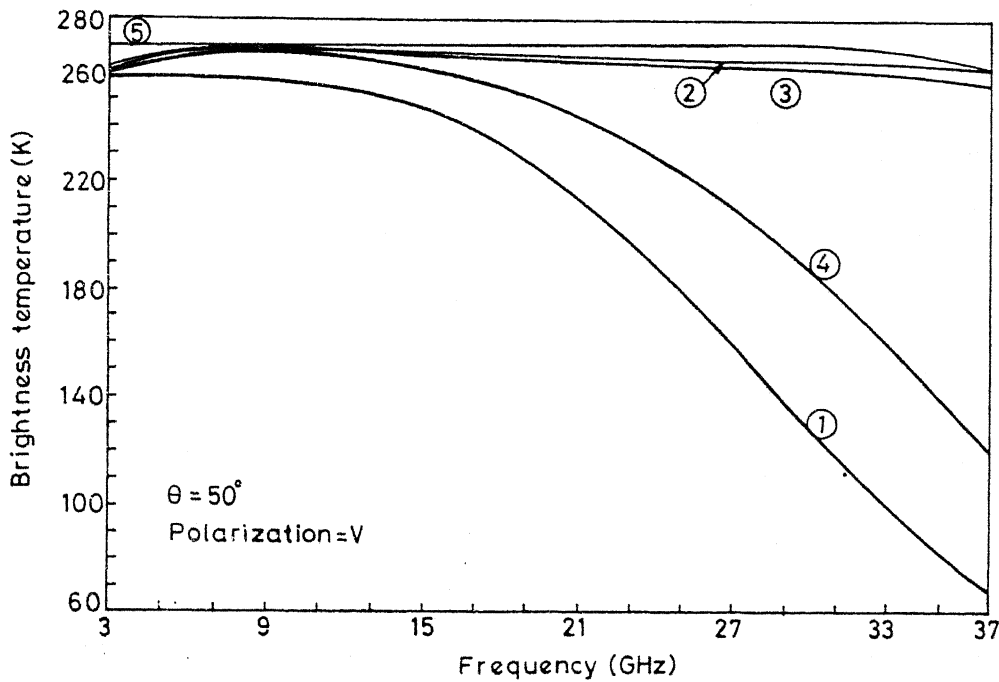
Frequency response of brightness temperature of yearly and multi-layered snowpacks charecterized by different wetness conditions in horizontal (Fig. 4.22) and vertical polarization (Fig. 4.23).

67

cycles.

The angular dependence of brightness temperature is shown in Figure 4.24 at 19 GHz frequency for the models given in the legend. The multi-layered models (1) and (2) are the representative of the early stage of melting and refreezing cycles of type 1 and 2 respectively, whereas model (3) is a representative of yearly snowpack in which the snow layer is wet. The brightness temperature contrast in horizontal and vertical polarizations $(T_{BV} - T_{BH})$ is very small for partially or completely wet snowpacks as compared to that of dry snowpacks (from Figures 4.21 and 4.24). This difference is almost same for the models 1, 2 and 3 (Figure 4.24). It can be inferred from the Figure 4.24 that the brewster angle (the angle at which the brightness temperature is maximum) is lower for multiyear snowpacks as compared to that of yearly snowpacks.

In order to study the effect of roughness of multi-layered snow surfaces, the brightness temperature behaviour with frequency is shown in Figure 4.25 for the models given in the legend at 50° look angle. The surface height variation of rough surface is taken to be 1 cm. For the snowpack, in which the top surface is rough, brightness temperature is higher as compared to that of smooth surface in 1-37 GHz frequency range. The variation in brightness temperature due to rough surface is pronounced in horizontal polarization, whereas it remains same in vertical polarization at 50° look angle.

The angular dependence of brightness temperature at 25 GHz frequency for dry and wet snowpacks in both the conditions of plane and rough surfaces is shown in Figure 4.26. The variation in

68
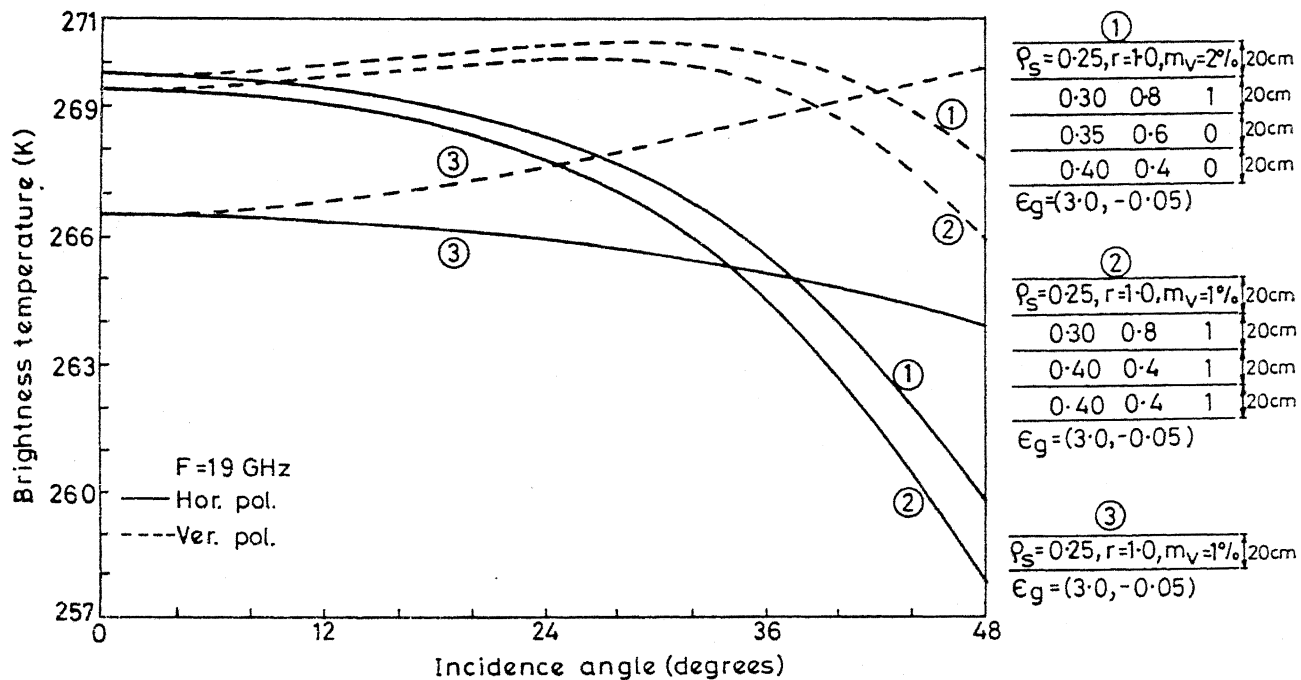
Fig. 4.24 Angular variation of brightness temperature of single and multi-layered wet snowpacks with varying wetness conditions.
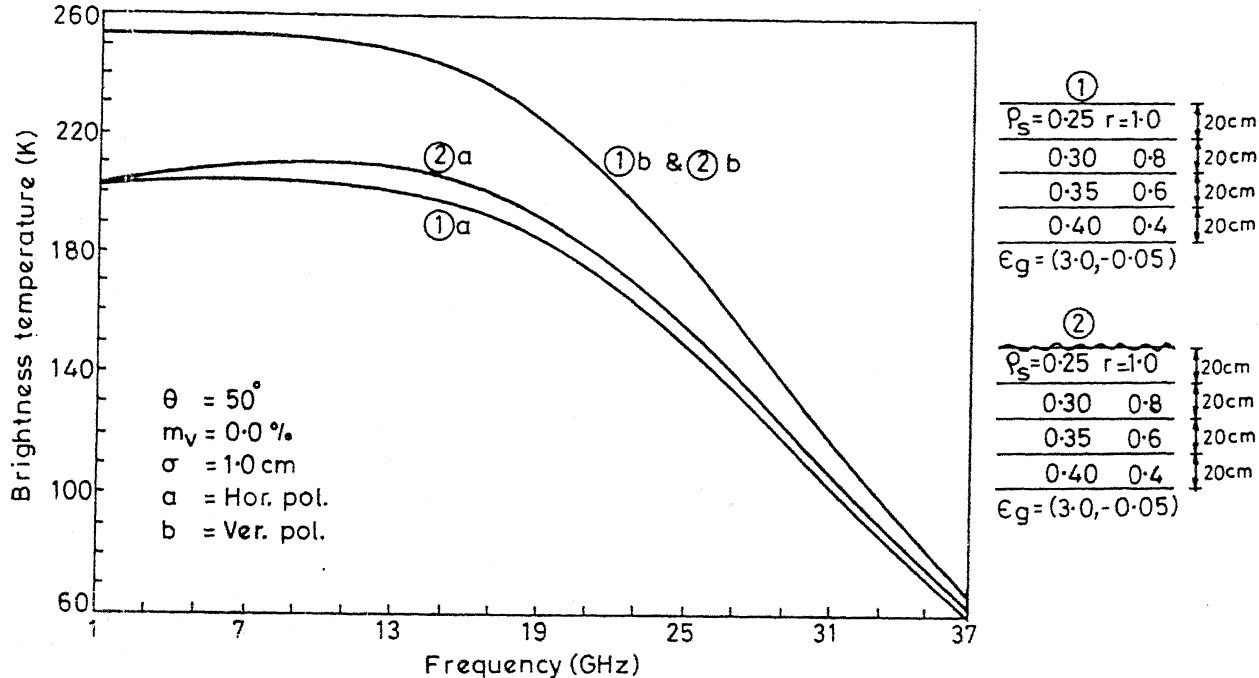
Fig. 4.25 Frequency response of brightness temperature for plane and rough top surfaces of dry multi-layered snowpack.
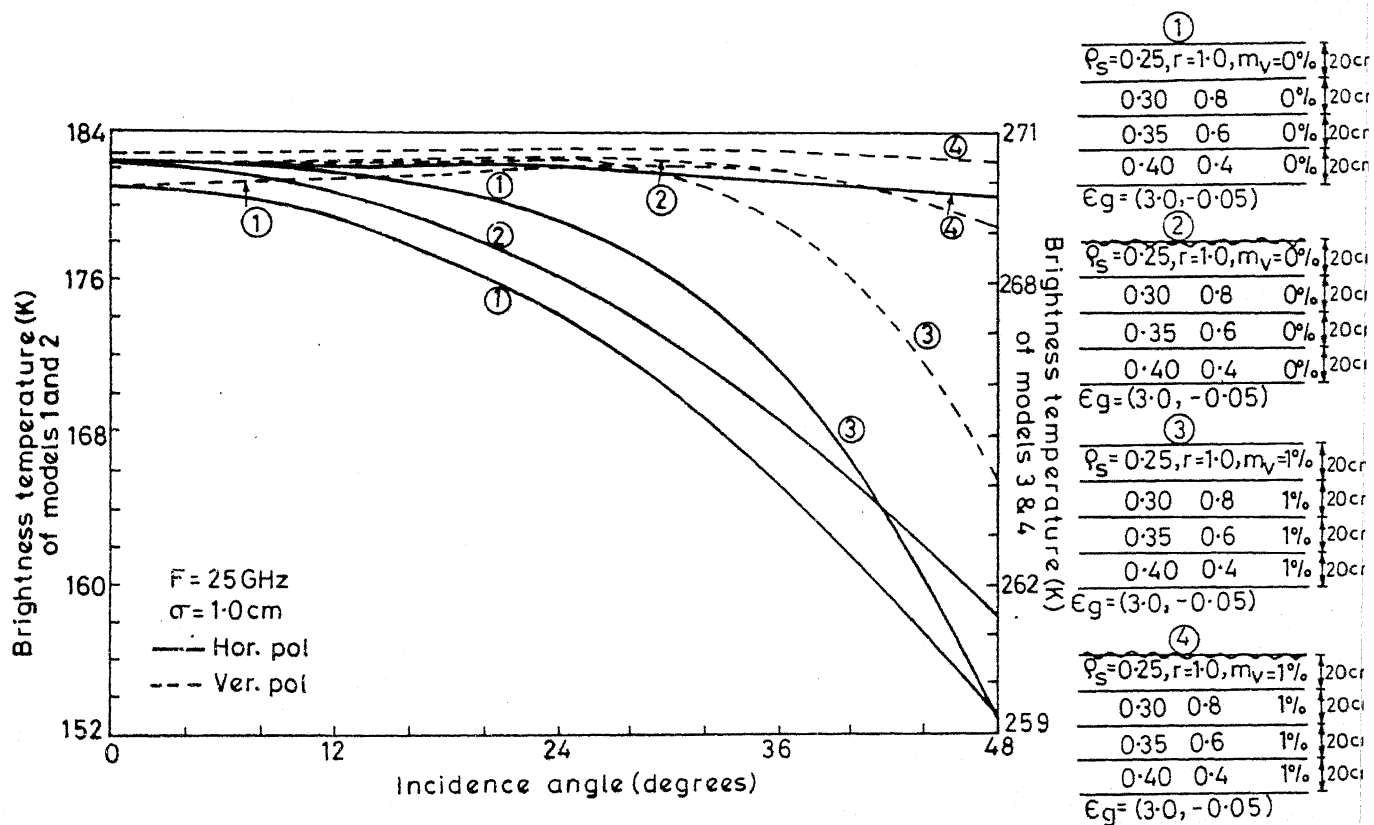
Fig. 4.26 Angular variation of brightness temperature for plane and rough top surfaces of dry and wet multi-layered snowpacks.

brightness temperature for smooth and rough surfaces increases with the increase of incidence angle for dry snowpacks in horizontal polarization and becomes negligible after 40° look angle in vertical polarization. In case of wet snowpack, the variation in brightness temperature for smooth and rough surfaces increases with the increase of incidence angle in both the polarizations. However, the polarization difference in brightness temperature ($T_{BV} - T_{BH}$) decreases as the surface of the snowpack becomes rough.

Therefore, the effect of surface roughness on microwave remote sensing response can be suppressed by the proper selection of sensor parameters such as frequency, incidence angle and polarization.

4.5 PASSIVE MICROWAVE REMOTE SENSING RESPONSE OF LAKE ICE

In polar and high-lattitude regions, the surface of the lake is often covered by an ice layer. The lake water is seldom pure as it contains dissolved salts and minerals as well as various chemicals, which increases its salinity. In order to estimate the thickness of ice layer overlying lake water, variation of brightness temperature as the function of ice thickness in horizontal polarization is shown in Figure 4.27 at the look angle of 50° for varying frequencies in both cases of pure and saline water. The average physical temperatures of ice layer and that of lake water are taken to be 272^OK. The brightness temperature of lake water (i.e. when d=0, where d is the thickness of ice layer) is lower than that of lake ice. The brightness temperature increases with the increase of frequency and ice thickness. The brightness temperature shows increasing trend with increase of

71
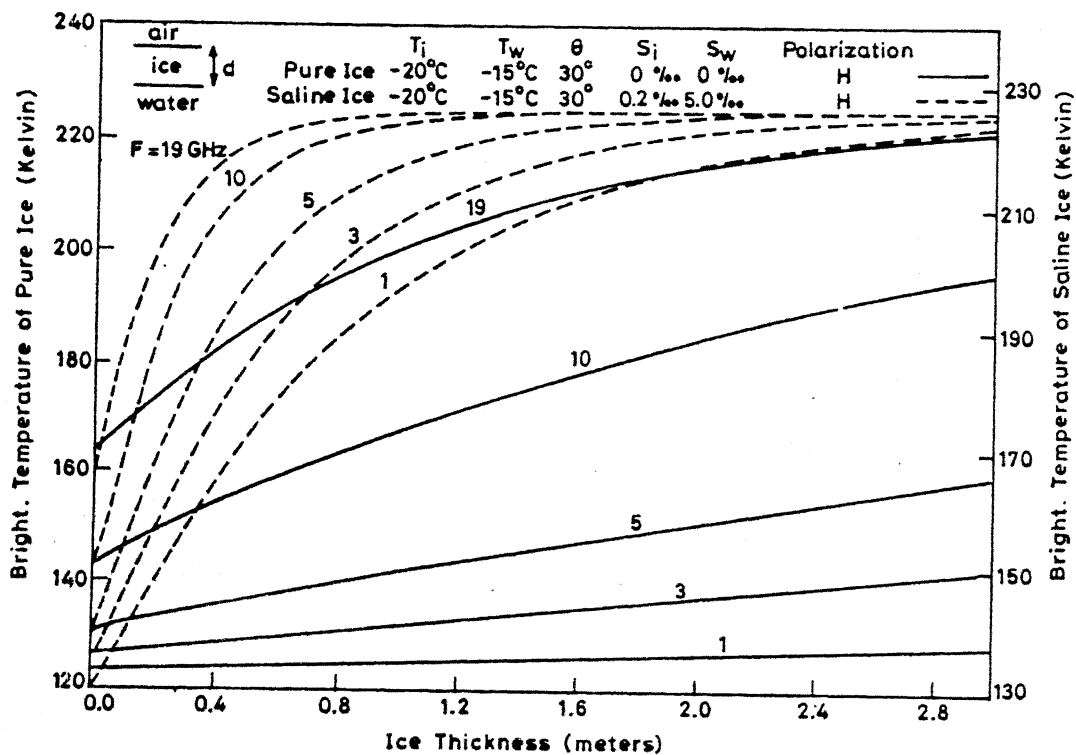
Fig. 4.27 Variation of brightness temperature with lake ice thickness.
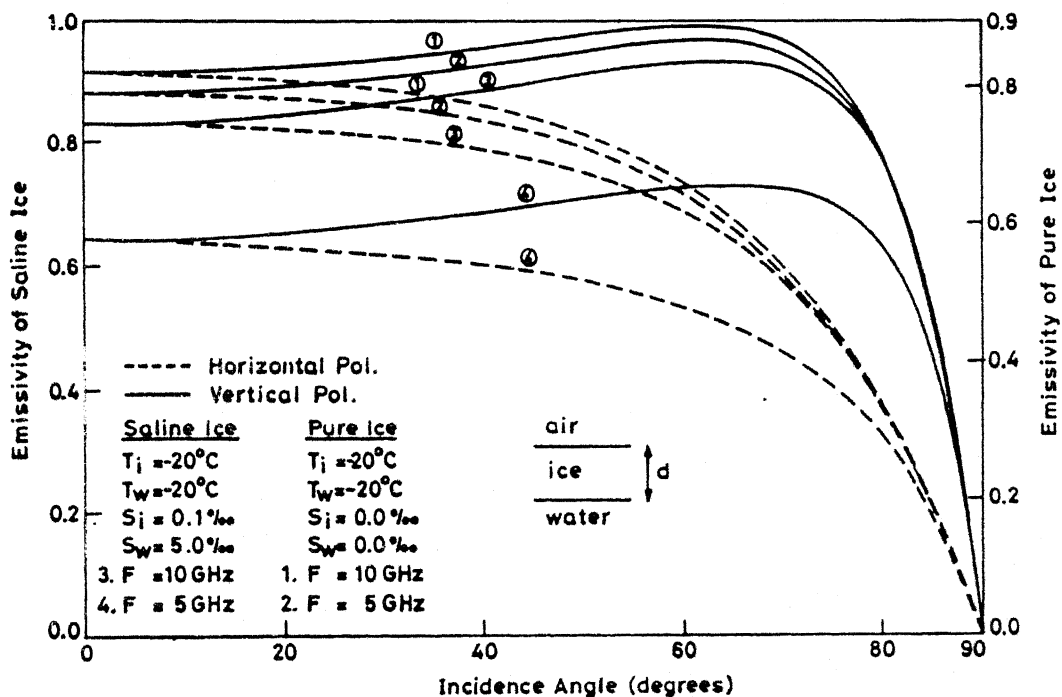
Fig. 4.28. Angular response of brightness temperature of lake ice at 5 and 10 GHz frequency.

frequency, the trend is more pronounced for saline ice than for pure ice. The brightness temperature of saline ice is higher as compared to that of pure ice for a particular frequency and ice thickness. For saline ice, the brightness temperature first increases rapidly with the increase of ice thickness and becomes constant after an optimum thickness for a particular frquency. Usually, lake water is never pure, therfore, it is clear from the Figure 4.27 that the frequency of 5 GHz will be most suitable for the estimation of lake ice thickness.

The angular dependence of emissivity of lake ice at 5 and 10 GHz is shown in Figure 4.28. The emissivity of pure and saline ice decreases with the increase of incidence angle in horizontal polarization, and increases in vertical polarization. The variation in brightness temperature for pure and saline ice decreases with the increasing look angle in horizntal polarization. Therefore, incidence angle of 0° will prove to be more advantageous.

Generally, the surface of lake ice is overlain by the snow layer, which modifies the emission behaviour of lake ice. If the snow layer is dry, of low density and has small ice particles, it will appear transparent electromagnetically for microwaves. However, the presence of wet snow will mask the emission from the underlying ice layer. Therefore in sensing the lake ice thickness, lower frequencies must be used to suppress the effect of snow layer on top.

73

CHAPTER 5

CONCLUSION

The snowfall is a frequent phenomenon for most of the year in the mid- and high-lattitude, and mountaineous regions. Due to continuous snowfall, snow accumulates on the surface and forms a thick layer. In the polar regions, the yearly accumulated snow piles up and forms a large mass of snow and ice. The physical and electromagnetic characteristics of the snow or ice varies with depth. Timely information about snow and ice cover is needed to predict the water supply, to anticipate flooding, to forecast crop yields and estimate freeze damage, to monitor climate, to obtain insights advantageous to military and foreign policy, and to guide winter sport activities. In this study, theoretical microwave remote sensing response of snow covered terrains has been computed. The numerical results show that the passive microwave remote sensing response of snow covered areas is highly dependent on the frequency, incidence angle and polarization of the microwave signal, and on the snowpack parameters.

The knowledge of dielectric constant is very important for the proper interpretation of microwave remote sensing data. The real and imaginary parts of complex dielectric constant of dry snow have been computed by using Polder-Van Santen two-phase mixing formula and that of wet snow by modified Debye-like model. The real part of dielectric constant of dry snow is the function of snow density and increases with the increase in snow density. The imaginary part increases with the increase of frequency,

temperature and snow density. The real and imaginary parts of dielectric constant of wet snow are the function of frequency, snow density and moisture content of snow. The imaginary part of dielectric constant of wet snow is considerably higher as compared to that of dry snow.

Scattering is the primary loss process in dry snow, whereas absorption becomes the dominant loss mechanism in wet snow due to significant increase in the imaginary part of dielectric constant when liquid water is present. The penetration depth of microwave signal depends upon frequency, snow density, snow particle size and free liquid water content of snow. The penetration depth is drastically reduced in the presence of even a small amount of liquid water and decreases with the increase in frequency, particle size and density of snow.

The brightness temperature of dry snow shows negative spectral slope, whereas wet snow and bare ground show positive slope. The wet snow can be discriminated from bare ground by measuring the brightness temperature contrast in vertical and horizontal polarizations at 50° incidence angle. It is concluded that the multifrequency and multiplarization approaches can be used for the snow characterization.

The snow particle size increases significantly as the snow layer becomes wet, which creates ambiguity in estimating the snow thickness. For the average snow particles size, frequency range of 25-37 GHz is most suited for obtaining the dry snow thickness information. The thickness of wet snow can not be determined due to the limited penetration depth of microwave signals in the presence of water. The diurnal fluctuation in

brightness temperature can be used to detect the onset of snowmelt, which is a very useful parameter for predicting the timing of runoff from a river basin. The free liquid water content of snow can be estimated accurately at lower frequencies. The effect of roughness is almost eliminated in vertical polarization at 50° look angle.

Snow generally accumulates in a layered structure and physical parameters of each layer change with depth and time. Therefore, the dielectric constant is also changed accordingly, which causes the brightness temperature of multi-layered models to change when compared to that of two-layered models. By the use of proper frequency and incidence angle, the number of layers present as well as the characteristics of each layer in a snowpack can be determined which can be used in monitoring melting and refreezing cycles of snow covered terrains. Our results also show that the lake ice thickness can be estimated by using microwave signal of about 5 GHz frequency.

The present study of microwave remote sensing of snow covered terrains suggests that the multi-channel microwave radiometers operating near 37, 25 and 5 GHz may prove to be ideal. The look angle of 50° seems to be reasonable for determining the the maximum information about the snowpacks.

The Indian Space Research Organization, Bangalore is planning to launch remote sensing satellites with microwave sensors on board in early nineties. The results discussed here will be useful in the development of appropriate microwave sensors and in the accurate interpretation of microwave remote sensing data of snow covered regions.

The data on dielectric constant of ice, and dry and wet snow are almost non-existant in microwave frequency range. Therefore, detailed experimental studies must be carried out to study the behaviour of dielectric properties of pure ice, and dry and wet snow in the VHF and microwave ranges.

REFERENCES

Burke, H.H.K., Bowley, C.J., and Barnes, C.J. (1984), Determination of snowpack properties from sattelite passive microwave measurement, Remote Sens. Environ., 15, pp. 1-20.

Carter, D.J. (1986), The remote sensing, Kogan Page Ltd., London.

Chang, A.T.C., Gloersen, P., Schmugge, T., Wilheit, T.T., and Zwally, H.J. (1976), Microwave emission from snow and glacier ice, J. Glaciol., 16, pp. 23-39.

Choudhury, T.J., Schmugge, T., Chang, A., and Newton, R.W. (1979), Effect of surface roughness on the microwave emission from soils, J. Geophys. Res., 84, pp. 5699-5706.

Colbeck, S.C. (1982), The geometry and permittivity of snow at high frequencies, J. Appl. Phys., 53, pp. 4495-4500.

Cumming, W. (1952), The dielectric properties of ice and snow at 3.2 cm, J. Appl. Phys., 23, pp. 768-773.

Dobson, M.C., Ulaby, F.T., Hallikainen, M., and El-Rayes, M. (1985), Microwave dielectric behaviour of wet soil-part II : four component dielectric mixing models, IEEE Trans. Geosci. Remote

Sensing, GE-23, pp. 35-46.

Earth Observing System Reports, II f (published by NASA).

Evans, S. (1965), Dielectric properties of ice and snow - a review, J. Glaciol., 5, pp. 773-792.

Foster, J.L., Hall, D.K., Chang A.T.C., and Rango A. (1984), An overview of passive microwave snow research and results, Rev. Geophys. and Space Phys., 22, pp. 195-208.

Frankenstein, G. and Garner, R. (1967), Equations for determining the brine volume of sea ice from -0.5 $^{\circ}$C to -22.9 $^{\circ}$C, J. Glaciol., 6, pp. 943-947.

Glen, J.W., and Paren P.G. (1975), The electrical properties of snow and ice, J. Glaciol., 15, pp. 15-38.

Grant, E., Buchanan, T., and Cook, T. (1957), Dielectric behaviour of water at microwave frequencies, J. Chem. Phys., 26, pp. 156-161.

Hall, D.K., Foster, J.L., Chang A.T.C., and Rango A. (1981), Fresh water ice thickness observations using passive microwave sensors, IEEE Trans. Geosci. Remote Sensing, GE-19, pp. 189-192.

Hallikainen, M., Ulaby, F.T., and Abdelrazik, M. (1982), Measurements of the dielectric properties of snow in the 4-18 GHz

frequency range, Proc. 12th European Microwave Conf., Helsinki, 13-17 Sept.

Hallikainen, M., Ulaby, F.T., and Abdelrazik, L. (1983), Modelling of dielectric behaviour of wet snow in the 4-18 GHz range, IEEE Intl. Geosci. Remote Sensing Symp. (IGARSS' 84) Digest, San Francisco, CA, 31st Aug. - 2nd Sept.

Hallikainen, M.T., Ulaby, F.T., and Abdelrazik, L. (1984a), The dielectric behaviour of snow in the 3-37 GHz range, IEEE Intl. Geosci. Remote Sensing Symp. (IGARSS'84) Digest, Straspourg, France, 27-30 Aug., pp. 169-176.

Hallikainen, M.T., Ulaby, F.T., and Abdelrazik, M. (1986), Dielectric properties of snow in the 3 to 37 GHz range, IEEE Trans. Antennas and Propagation, AP-34, 1, 1329-1340.

Hoekstra, P., and Cappillino, P. (1971), Dielectric properties of sea and sodium chloride ice at UHF and microwave frequencies, J. Geophys. Res., 76, pp. 4922-4931.

Kong, J.A., Shin, R., Shine, J.C., and Tsang, L., (1979), Theory and experiment for passive microwave remote sensing of snowpacks, J. Geophys. Res., 84, pp. 5669-5673.

Matzler, C. (1987), Applications of the interaction of microwaves with the natural snow cover, Remote Sensing Reviews, 2, pp. 259-387.

Rankin, D., and Singh, R.P. (1985), Effect of clay and salinity on the dielectric properties of rock, J. Geophys. Res., 90, 8793-8800.

Schanda, E., Matzler, C., and Kunzi, K. (1983), Microwave remote sensing of snow cover, Int. J. Remote Sensing, 4, pp. 149-158.

Schultz, G.A. (1988), Remote sensing in hydrology, J. Hydrology, 100, pp. 239-265.

Singh, R.P. (1984), Dielectric properties and microwave remote sensing, Adv. Space Res., 4, pp. 97-101.

Singh, R.P., Kumar, V., Srivastav, S.K. (1989), Use of microwave remote sensing in salinity estimation, Intl. J. Remote Sensing (In Press).

Stiles, W.H., and Ulaby, F.T. (1980 b), The active and passive microwave response to snow parameters, Part I: Wetness, J. Geophys. Res., 85, pp. 1037-1044.

Stiles, W.H., and Ulaby, F.T. (1981), Dielectric properties of snow, NASA Contract Rep., CR166764.

Stogryn, A. (1971), Equations for calculating the dielectric constant of saline water, IEEE Trans. Microwave Theory Techn. MIT-19, pp. 733-736.

Swift, C.T., Jones, W.L., Harrington, R.F., Fedors, J.C., and

Couch, R.H. (1980), Microwave radar and radoimetric remote sensing measurements of lake ice, Geophys. Res. Letters, 7, pp. 243-246.

Tiuri, M.E. (1982), Theoretical and experimental studies of microwave signatures of snow, IEEE Trans. Geosci. Remote Sensing, GE-20, pp.51-57.

Ulaby, F.T., and Stiles, W.H. (1980), The active and passive microwave response to snow parameters, part II : water equivalent of dry snow, J. Geophys. Res., 85, pp. 1045-1049.

Ulaby, F.T., and Stiles, W.H. (1981), Microwave response of snow, Adv. Space Res., 1, pp. 131-149.

Ulaby, F.T., Moore, R.K., and Fung, A.K. (1981), Microwave remote sensing, 1 and III, Artech House, MA.

Vant, M.R., and Ramseier, R.O., and Makios, V. (1978), The complex dielectric constant of sea ice at 10 and 35 GHz, J. App. Phys., 49, pp. 1264-1280.

APPENDIX - A1

```
C***********************************************************************
C******   THIS PROGRAM COMPUTES THE REAL AND IMAGINARY PARTS
C******   OF DIELECTRIC CONSTANT OF DRY SNOW / PROGRAMMED BY
C******   SUSHIL K.SRIVASTAV /
C***********************************************************************
C******   VARIABLES  INVOLVED ARE FREQUENCY, REAL  AND  IMAGINARY
C******   PARTS OF DIELECTRIC CONSTANT OF PURE ICE, AND DENSITY
C******   OF DRY SNOW AND PURE ICE.
C***********************************************************************
C******   F1 = FREQUENCY IN GHz
C******   EPICPX = DIELECTRIC LOSS FACTOR OF PURE ICE
C******   RHOS = DENSITY OF DRY SNOW
C******   RHOI = DENSITY OF PURE ICE
C******   VI = VOLUME FRACTION OF ICE
C******   EPIRL = DIELECTRIC PERMITTIVITY OF PURE ICE
C******   EDSRL = DIELECTRIC PERMITTIVITY OF DRY SNOW
C******   EDSCX = DIELECTRIC LOSS FACTOR OF DRY SNOW
C***********************************************************************
          DIMENSION F1(100),EPICPX(100)
          REAL F1,F,RHOS,RHOI,VI,EDSRL,BC,CC,DC,EC,EDSCX
          OPEN(UNIT=26,FILE='M5.DAT')
          OPEN(UNIT=27,FILE='F4.RES')
          PI=3.142857
          RHOI=0.916
          EPIRL=3.15
          DO 200 IRS=10,50,10
          DO 100 I=1,37
          READ(26,*)F1(I),EPICPX(I)
          F=F1(I)*1.0E09
          RHOS=IRS/100.0
          VI=RHOS/RHOI
          EDSRL=(1.0+0.508*RHOS)**3
          BC=EDSRL**2
          CC=2.0*EDSRL
          DC=3.15+CC
          EC=3.15+(2.0*BC)
          EDSCPX=3.0*VI*EPICPX(I)*BC*(CC+1.0)/(DC*EC)
          WRITE(27,*)EDSRL,EDSCPX
100       CONTINUE
200       CONTINUE
          STOP
          END
C******   ----------------------------------------------------------
```

APPENDIX - A2

```
C*******************************************************************
C******   THE   PROGRAM   COMPUTES   THE   REAL   AND   IMAGINARY PARTS
C******   OF   THE   COMPLEX   DIELECTRIC CONSTANT   OF   WET   SNOW
C******   BY   USING   DEBYE-LIKE   MODEL / PROGRAMED BY SUSHIL K.
C******   SRIVASTAV /
C*******************************************************************
C******   VARIABLES INVOLVED ARE FREQUENCY, DIELECTRIC LOSS FACTOR
C******   OF PURE ICE, SNOW WETNESS, AND DENSITY OF WET SNOW.
C*******************************************************************
C******   F1 = FREQUENCY IN Hz
C******   EPICPX = DIELECTRIC LOSS FACTOR OF PURE ICE
C******   MV = VOLUMETRIC WATER CONTENT IN PERCENTAGE
C******   RHOS = DENSITY OF WET SNOW IN C.G.S. UNITS
C******   RHOI = DENSITY OF ICE IN C.G.S. UNITS
C******   EWSRL = DIELECTRIC PERMITTIVITY OF WET SNOW
C******   EWSCX = DIELECTRIC LOSS FACTOR OF WET SNOW
C*******************************************************************
          DIMENSION F1(200),EPICPX(200),EWSRL(200),EWSCX(200)
          REAL F1,EPICPX,FREQ,RHOS,RHOI,MV,A1,A2,B1,A,B,C,X,F0,Z,EWSRL,EU
          OPEN(UNIT=21,FILE='A1.DAT')
          OPEN(UNIT=25,FILE='A6.RES')
          PI=3.142857
          RHOS=0.25
          RHOI=0.916
          DO 400 IM=1,9,2
          DO 300 I=1,37
          READ(21,*)F1(I),EPICPX(I)
          MV=IM/1.0
          FREQ=37.0
          A1=0.78+0.03*FREQ-0.58*1.0E-03*(FREQ**2)
          A2=0.97-0.39*FREQ*1.0E-02+0.39*1.0E-03*(FREQ**2)
          B1=0.31-0.05*FREQ+0.87*1.0E-03*(FREQ**2)
          A=1.0+(1.83*RHOS)+(0.02*A1*(MV**1.015))+B1
          B=0.073*A1
          C=0.073*A2
          X=1.31
          F0=9.07
          Z=FREQ/F0
          EWSRL(I)=A+((B*(MV**X))/(1.0+Z*Z))
          EWSCX(I)=(C*Z*MV**X)/(1.0+Z*Z)
          WRITE(25,*)IM,EWSRL(I),EWSCX(I)
300       CONTINUE
400       CONTINUE
          STOP
          END
C******   --------------------------------------------------------
```

APPENDIX - A3

```
C*******************************************************************
C****** THE   PROGRAM   COMPUTES   THE   REAL   AND   IMAGINARY   PART
C****** OF   THE   COMPLEX   DIELECTRIC   CONSTANT   OF   PURE   WATER
C****** BY   USING   DEBYE   EQUATIONS / PROGRAMMED BY SUSHIL K.
C****** SRIVASTAV /
*******************************************************************
C****** VARIABLES INVOLVED ARE FREQUENCY AND TEMPERATURE.
C*******************************************************************
C****** F1= FREQUENCY IN GHz
C****** T = PHYSICAL TEMPERATURE OF WATER
C****** EPWRL = DIELECTRIC PERMITTIVITY OF PURE WATER
C****** EPWCX = DIELECTRIC LOSS FACTOR OF PURE WATER
C*******************************************************************
        DIMENSION F1(100),EPWRL(100),EPWCX(100)
        REAL F1,F,T,EWINF,EWO,X,A,B,TOW,C,D,EPWRL,EPWCX
        OPEN(UNIT=22,FILE='FREQ.DAT')
        OPEN(UNIT=23,FILE='A2.dat')
        PI=3.142857
        DO 100 IT=1,26
        DO 100 I=1,28
        T=IT-1.0
        READ(22,*)F1(I)
        F=F1(I)*1.0E09
        EWINF=4.9
        EWO=88.045-0.4147*T+6.295E-04*T*T+1.075E-5*T**3
        X=2.0*PI
        A=1.1109E-10-3.824E-12*T
        B=6.938E-14*T*T-5.096E-16*T**3
        TOW=(A+B)/X
        C=(X*F*TOW)**2
        D=1.0+C
        EPWRL(I)=EWINF+((EWO-EWINF)/D)
        EPWCX(I)=(X*F*TOW*(EWO-EWINF))/D
        WRITE(23,*)F1(I),EPWRL(I),EPWCX(I)
100     CONTINUE
200     CONTINUE
        STOP
        END
```

APPENDIX-A4

```
C************************************************************************
C****** THIS PROGRAM COMPUTES THE REAL AND IMAGINARY PART
C****** OF THE COMPLEX DIELECTRIC CONSTANT OF SALINE
C****** WATER BY USING STOGRYN'S FORMULATION / PROGRAMMED
C****** BY SUSHIL K. SRIVASTAV /
C************************************************************************
C****** VARIABLES INVOLVED ARE FREQUENCY, TEMP. AND SALINITY.
C************************************************************************
C****** F1= FREQUENCY IN GHz
C****** EPO = PERMITTIVITY OF FREE SPACE
C****** T = PHYSICAL TEMPERATURE OF SALINE WATER
C****** S = SALINITY OF WATER
C****** EPWRL = PERMITTIVITY OF SALINE WATER
C****** EPWCX = DIELCTRIC LOSS FACTOR OF SALINE WATER
C************************************************************************
        DIMENSION F1(100),EPWRL(100),EPWCX(100)
        REAL T,S,F1,F,EPO,EPTO,A,B,ATS,EPTS,TM,TO,C,D,BTS
        REAL TOTS,DEL,E,G,PHI,SIG,SIGMI,XX,EPWRL,EPWCX
        OPEN(UNIT=24,FILE='FREQ.DAT')
        OPEN(UNIT=25,FILE='B1.DAT')
        PI=3.142857
        EPO=8.854E-12
        DO 200 I=1,28
        T=25.0
        S=35.0
        READ(24,*)F1(I)
        F=F1(I)*1.0E09
        EPTO=87.134-1.949E-1*T-1.276E-2*T*T+2.491E-4*T**3
        A=1.0+1.613E-5*T*S-3.656E-3*S
        B=3.210E-5*S*S-4.232E-7*S**3
        ATS=A+B
        EPTS=EPTO*ATS
        TM=1.1109E-10-3.824E-12*T+6.938E-14*T*T-5.096E-16*T**3
        TO=TM/(2.0*PI)
        C=1.0+2.282E-5*T*S-7.638E-4*S
        D=7.760E-6*S*S-1.105E-8*S**3
        BTS=C-D
        TOTS=TO*BTS
        DEL=25.0-T
        E=2.033E-2+1.266E-4*DEL+2.464E-6*DEL*DEL
        G=S*(1.849E-5-2.551E-7*DEL+2.551E-8*DEL*DEL)
        PHI=DEL*(E-G)
        SIG=S*(0.18252-1.4619E-3*S+2.093E-5*S*S-1.282E-7*S**3)
        SIGMI=SIG*EXP(-PHI)
        XX=2.0*PI*F*TOTS
        AA1=(XX*(EPTS-4.9)/(1.0+XX*XX))
```

```
        BB1=(SIGMI/(2.0*PI*F*EP0))
        EPWRL(I)=4.9+((EPTS-4.9)/(1.0+XX*XX))
        EPWCX(I)=AA1+BB1
        WRITE(25,*)F1(I),EPWRL(I),EPWCX(I)
200     CONTINUE
        STOP
        END
```

APPENDIX -A5

```
C*******************************************************************
C******   THE  PROGRAM  COMPUTES  THE  ABSORPTION,  SCATTERING AND
C******   EXTINCTION  COEFFICIENT,  AND  DEPTH  OF  PENETRATION OF
C******   MICROWAVES  IN  DRY  AND  WET  SNOW  BY  USING  RAYLEIGH
C******   EXPRESSIONS / PROGRAMMED BY SUSHIL K. SRIVASTAV /
C*******************************************************************
C******   VARIABLES INVOLVED ARE FREQUENCY, TEMPERATURE, REAL AND
C******   IMAGINARY PART OF COMPLEX DIELECTRIC CONSTANT OF PURE ICE,
C******   DENSITY OF SNOW AND PURE ICE, SNOW PARTICLE SIZE, AND
C******   SNOW WETNESS.
C*******************************************************************
C******   F1 = FREQUENCY IN Hz
C******   EPICPX = DIELECTRIC LOSS FACTOR OF PURE ICE
C******   R = RADIUS OF SNOW PARTICLES IN METRES
C******   MV = SNOW WETNESS EXPRESSED IN PERCENTAGE
C******   RHOI = DENSITY OF PURE ICE IN C.G.S. UNIT
C******   RHOS = DENSITY OF SNOW IN C.G.S. UNIT
C******   VI = VOLUME FRACTION OF ICE
C******   EDSRL = DIELECTRIC PERMITTIVITY OF DRY SNOW
C******   EDSCPX = DIELECTRIC LOSS FACTOR OF DRY SNOW
C******   EWSRL = DIELECTRIC PERMITTIVITY OF WET SNOW
C******   EWSCPX = DIELECTRIC LOSS FACTOR OF WET SNOW
C******   EPB = COMPLEX DIELECTRIC CONSTANT OF BACKGROUND MEDIUM
C******   EPWRL = DIELECTRIC PERMITTIVITY OF PURE WATER
C******   EPWCX = DIELECTRIC LOSS FACTOR OF PURE WATER
C******   EPSR = DIELECTRIC CONSTANT OF SNOW RELATIVE TO THAT
C******   OF THE BACKGROUND MEDIUM
C******   KAI = ABSORTION COEFFICIENT OF ICE PARTICLES
C******   KAB = ABSORPTION COEFFICIENT OF BACKGROUND MEDIUM
C******   KA = TOTAL ABSORPTION COEFFICIENT (KAI+KAB)OF SNOW  MEDIUM
C******   KS = SCATTERING COEFFICIENT OF SNOW MEDIUM
C******   KE = EXTINCTION COEFFICIENT OF SNOW MEDIUM
C******   DELTP = PENETRATION DEPTH
C*******************************************************************
        DIMENSION F1(500),EPICPX(500)
        REAL F1,FREQ,R,R1,RHOI,RHOS,VI,EDSRL,BC,CC,DC,EC,EPICPX
        REAL EDSCPX,EWSRL,EWSCPX,A2,B1,A,B,C,X,X1,F0,Z,CA,DA
        REAL Z,EWINF,EWO,TOW,EPWRL,EPWCX,ALB,DELTP
        REAL K1,K2,KA,KE,KS,L,MV,LMDAO,KAI,KAB,KA1,KS1,KE1
        COMPLEX EP2,AK,EPSR,EPB,EPW,A1
        OPEN(UNIT=21,FILE='SKS1.DAT')
        OPEN(UNIT=25,FILE='SKS1.RES')
        PI=3.142857
        RHOI=0.916
        DO 500 IM=1,13,1
        DO 400 I=1,37
```

```
      READ(21,*)F1(I),EPICPX(I)
      FREQ=F1(I)/1.0E09
      MV=(IM-1.0)
      DO 300 IR=20,500,10
      R=(IR/100.0)*1.0E-03
      R1=R*1.0E03
      DO 200 IRS=10,39,1
      RHOS=(IRS/100.0)
      K1=(2.0*PI*F1(I))/3.0E08
      VI=RHOS/RHOI
      IF(MV.GT.0.0)GO TO 15
      EDSRL=(1.0+0.508*RHOS)**3
      BC=EDSRL**2
      CC=2.0*EDSRL
      DC=3.15+CC
      EC=3.15+(2.0*BC)
      EDSCPX=3.0*VI*EPICPX(I)*BC*(CC+1.0)/(DC*EC)
      EP2=CMPLX(EDSRL,-EDSCPX)
      EPB=CMPLX(1.0,-0.0)
      GO TO 20
15    A1=0.78+0.03*FREQ-0.58*1.0E-03*(FREQ**2)
      A2=0.97-0.39*FREQ*1.0E-02+0.39*1.0E-03*(FREQ**2)
      B1=0.31-0.05*FREQ+0.87*1.0E-03*(FREQ**2)
      A=1.0+(1.83*RHOS)+(0.02*A1*(MV**1.015))+B1
      B=0.073*A1
      C=0.073*A2
      X=1.31
      F0=9.07
      Z=FREQ/F0
      EWSRL=A+((B*(MV**X))/(1.0+Z*Z))
      EWSCPX=(C*Z*MV**X)/(1.0+Z*Z)
      EP2=CMPLX(EWSRL,-EWSCPX)
      T=-1.0
      EWINF=4.9
      EW0=88.045-0.4147*T+6.295E-04*T*T+1.075E-05*T**3
      X1=2.0*PI
      A=1.1109E-10-3.824E-12*T
      B=6.938E-14*T*T-5.096E-16*T**3
      TOW=(A+B)/X1
      C=(X*F1(I)*TOW)**2
      D=1.0+C
      EPWRL=EWINF+((EW0-EWINF)/D)
      EPWCX=(X1*F1(I)*TOW*(EW0-EWINF))/D
      EPW=CMPLX(EPWRL,-EPWCX)
      A1=(1.0-(3.0*MV/100.0))*(EPW-1.0)-1.0
      EPB=(-A1+CSQRT(A1*A1+8.0*EPW))/4.0
20    LMDA0=3.0E08/F1(I)
      EPSR=EP2/EPB
      AK=(EPSR-1.0)/(EPSR+2.0)
```

```
        Z=AIMAG(-AK)
        KAI=(6.0*PI*VI*Z*CABS(EPB))/LMDA0
        IF(MV.EQ.0.0)GO TO 22
        KAB=2.0*K1*(1.0-VI)*ABS(AIMAG(CSQRT(EPB)))
        GO TO 23
22      KAB=0.0
23      KA=KAI+KAB
        CA=32.0*PI**4*R**3*VI*(CABS(AK))**2*CABS(EPB)**4
        DA=LMDA0**4
        KS=CA/DA
        KE=KA+KS
        ALB=KS/KE
        DELTP=1.0/KE
        WRITE(25,*)F1(I),MV,R1,RHOS,KA,KS,KE,DELTP
200     CONTINUE
300     CONTINUE
400     CONTINUE
500     CONTINUE
        STOP
        END
C******  -----------------------------------------------------
```

APPENDIX - A6

```
C********************************************************************
C******     THIS PROGRAM  COMPUTES  THE BRIGHTNESS TEMPERATURE OF
C******     TWO-LAYERED MODEL / PROGRAMMED BY SUSHIL K. SRIVASTAV
C********************************************************************
C******     VARIABLES  INVOLVED ARE FREQUENCY, REAL  AND  IMAGINARY
C******     PARTS OF DIELECTRIC CONSTANT OF PURE ICE, DENSITY OF
C******     PURE ICE AND SNOW,  RADIUS OF SNOW PARTICLES, LIQUID
C******     WATER CONTENT OF SNOW, AND TEMPERATURE.
C********************************************************************
C******     F1 = FREQUENCY IN GHz
C******     EPICPX = DIELECTRIC LOSS FACTOR OF PURE ICE
C******     R = RADIUS OF SNOW PARTICLES
C******     MV = SNOW LIQUID WATER CONTENT
C******     RHOI = DENSITY OF PURE ICE
C******     RHOS = DENSITY OF SNOW
C******     VI = VOLUME FRACTION OF ICE
C******     EPB = COMPLEX DIELECTRIC CONSTANT OF BACKGROUND MEDIUM
C******     KAI = ABSORPTION COEFFICIENT OF ICE PARTICLES
C******     KAB = ABSORPTION COEFFICIENT OF BACKGROUND MEDIUM
C******     KS = SCATTERING COEFFICIENT OF THE MEDIUM
C******     THETO = ANGLE OF INCIDENCE
C******     EP3 = COMPLEX DIELETRIC CONSTANT OF GROUND MEDIUM
C********************************************************************
       DIMENSION F1(200),EPICPX(200)
       REAL K1,K2,KA,KE,KS,L,MV,LMDA0,KAI,KAB,MV1
       COMPLEX EP2,EP3,R2V,R1V,R2H,R1H,AK,EPSR,EPB,EPW,A1
       OPEN(UNIT=21,FILE='SKS6.DAT')
       OPEN(UNIT=22,FILE='S18.RES')
       OPEN(UNIT=25,FILE='S14.RES')
       DO 400 IM=1,2
       DO 300 I=1,35
       READ(21,*)F1(I),EPICPX(I)
       F=F1(I)*1.0E09
       TI=272.0
       TG=272.0
       D1=0.5
       D11=D1*100.0
       RHOS=0.25
       WE=D11*RHOS
       RHOI=0.916
       R=1.0*1.0E-03
       PI=3.142857
       FREQ=F/1.0E09
       K1=(2.0*PI*F)/3.0E08
       VI=RHOS/RHOI
       EP3=CMPLX(3.0,-0.05)
       IF(MV.GT.0.0)GO TO 15
```

```
      EDSRL=(1.0+0.508*RHOS)**3
      BC=EDSRL**2
      CC=2.0*EDSRL
      DC=3.15+CC
      EC=3.15+(2.0*BC)
      EDSCPX=3.0*VI*EPICPX(I)*BC*(CC+1.0)/(DC*EC)
      EP2=CMPLX(EDSRL,-EDSCPX)
      EPB=CMPLX(1.0,-0.0)
      GO TO 20
15    A1=0.78+0.03*FREQ-0.58*1.0E-03*(FREQ**2)
      A2=0.97-0.39*FREQ*1.0E-02+0.39*1.0E-03*(FREQ**2)
      B1=0.31-0.05*FREQ+0.87*1.0E-03*(FREQ**2)
      A=1.0+(1.83*RHOS)+(0.02*A1*(MV**1.015))+B1
      B=0.073*A1
      C=0.073*A2
      X=1.31
      F0=9.07
      Z=FREQ/F0
      EWSRL=A+((B*(MV**X))/(1.0+Z*Z))
      EWSCPX=(C*Z*MV**X)/(1.0+Z*Z)
      EP2=CMPLX(EWSRL,-EWSCPX)
      T=-1.0
      EWINF=4.9
      EWO=88.045-0.4147*T+6.295E-04*T*T+1.075E-05*T**3
      X=2.0*PI
      A=1.1109E-10-3.824E-12*T
      B=6.938E-14*T*T-5.096E-16*T**3
      TOW=(A+B)/X
      C=(X*F*TOW)**2
      D=1.0+C
      EPWRL=EWINF+((EWO-EWINF)/D)
      EPWCX=(X*F*TOW*(EWO-EWINF))/D
      EPW=CMPLX(EPWRL,-EPWCX)
      A1=(1.0-(3.0*MV/100.0))*(EPW-1.0)-1.0
      EPB=(-A1+CSQRT(A1*A1+8.0*EPW))/4.0
20    LMDA0=3.0E08/F
      EPSR=EP2/EPB
      AK=(EPSR-1.0)/(EPSR+2.0)
      Z=AIMAG(-AK)
      KAI=(6.0*PI*VI*Z*CABS(EPB))/LMDA0
      IF(MV.EQ.0.0)GO TO 22
      KAB=2.0*K1*(1.0-VI)*ABS(AIMAG(CSQRT(EPB)))
      GO TO 23
22    KAB=0.0
23    KA=KAI+KAB
      CA=32.0*PI**4*R**3*VI*(CABS(AK))**2*CABS(EPB)**4
      DA=LMDA0**4
      KS=CA/DA
```

```
       KE=KA+KS
       ALB=KS/KE
       THETO=0.0
30     THET1=THETO*PI/180.0
       THET2=ASIN(CABS(CSQRT(1.0/EP2))*SIN(THET1))
       THET3=ASIN(CABS(CSQRT(EP2/EP3))*SIN(THET2))
       L=EXP(KE*D1*1.0/COS(THET2))
       AMUO=4.0*PI*1.0E-07
       EPO=8.854E-12
       Z1=SQRT(AMUO/EPO)
       Z1V=Z1*COS(THET1)
       Z2V=(Z1*COS(THET2)/CSQRT(EP2))
       Z3V=(Z1*COS(THET3)/CSQRT(EP3))
       R2V=(Z2V-Z3V)/(Z2V+Z3V)
       R1V=(Z1V-Z2V)/(Z1V+Z2V)
       REFL2V=(CABS(R2V))**2
       REFL1V=(CABS(R1V))**2
       AA1=1.0-REFL1V
       BB1=1.0
       CC1=1.0+(REFL2V/L)
       DD1=1.0-(1.0/L)
       EE1=(1.0-ALB)
       FF1=((1.0-REFL2V)/L)
       EMISV=AA1*((CC1*DD1*EE1*TI)+FF1*TG)/BB1
       Z1H=Z1/COS(THET1)
       Z2H=(Z1/(COS(THET2)*CSQRT(EP2)))
       Z3H=(Z1/(COS(THET3)*CSQRT(EP3)))
       R2H=(Z3H-Z2H)/(Z3H+Z2H)
       R1H=(Z2H-Z1H)/(Z2H+Z1H)
       REFL2H=(CABS(R2H))**2
       REFL1H=(CABS(R1H))**2
       AA2=1.0-REFL1H
       BB2=1.0
       CC2=1.0+(REFL2H/L)
       DD2=1.0-(1.0/L)
       EE2=(1.0-ALB)
       FF2=((1.0-REFL2H)/L)
       EMISH=AA2*((CC2*DD2*EE2*TI)+FF2*TG)/BB2
       TBVMTBH=EMISV-EMISH
       WRITE(22,*)IM,F1(I),THETO,EMISV,EMISH
       THETO=THETO+4.0
       IF(THETO.LE.50.0)GO TO 30
300    CONTINUE
400    CONTINUE
       STOP
       END
C******  ---------------------------------------------------
```

APPENDIX - A7

```
C****************************************************************
C*****   THIS  PROGRAM  COMPUTES THE  BRIGHTNESS TEMPERATURE  OF
C*****   MULTI-LAYERED MODELS/PROGRAMMED BY SUSHIL K. SRIVASTAV.
C****************************************************************
C*****   VARIABLES   ARE SAME AS GIVEN IN THE   PROGRAM   FOR TWO-
C*****   LAYERED MODEL. SIG IS THE SURFACE HEIGHT VARIATION.
C****************************************************************

        DIMENSION F1(150),F(150),EPICPX(150),RHOS(150,10)
        DIMENSION R(150,10),H(150,10),EP(150,10),Z(150,10)
        DIMENSION KE(150,10),ALB(150,10),THET(150,10),X(150,10)
        DIMENSION REFLV(150,10),EMISV(150,10),RR1(150,10)
        DIMENSION EMIS1(150),TB1(150),KA(150,10),KS(150,10)
        DIMENSION L(150,10),ZV(150,10),RFL(10),R1(150,10)
        DIMENSION RR2(150,10),ZH(150,10),REFLH(150,10),Y(150,10)
        DIMENSION EMISH(150,10),EMIS2(150),TB2(150),MV(150,10)
        DIMENSION SIG(150,10),REF1H(150,10),REF1V(150,10),KAB(150,10)
        DIMENSION K(150,10),HDASH(150,10),FACT(150,10),KAI(150,10)
        DIMENSION MV1(150,10),EPW(150,10),EPB(150,10),EPSR(150,10)
        REAL L,K,KA,KS,KE,KAI,LMDAO,TB,MV,MV1,KAB
        COMPLEX EP,AK,ZV,ZH,AB,EPB,EPW,EPSR
        OPEN(UNIT=21,FILE='SKS6.DAT')
        OPEN(UNIT=22,FILE='SKS7.DAT')
        OPEN(UNIT=24,FILE='S26.RES')
        DO 700 I=1,115
        READ(21,*)F1(I),EPICPX(I)
        DO 600 J=2,5
        READ(22,*)RHOS(I,J),R1(I,J),H(I,J)
600     CONTINUE
700     CONTINUE
        PI=3.142857
        EPO=8.854E-12
        AMUO=4.0*PI*1.0E-07
        T=272.0
        C=3.0E08
        RHOI=0.916
        DO 550 I=1,1
        EP(I,1)=CMPLX(1.0,-0.0)
        EP(I,6)=CMPLX(3.5,-0.05)
        Z(I,1)=SQRT(AMUO/EPO)
550     CONTINUE
        DO 545 I=1,115
        DO 540 J=2,5
        SIG(I,1)=0.01
        SIG(I,J)=0.0
540     CONTINUE
545     CONTINUE
        DO 481 I=1,1
```

```
              DO 480 J=2,5
              MV(I,J)=1.0
480           CONTINUE
481           CONTINUE
              DO 500 I=1,1
              DO 400 J=2,5
              VI=RHOS(I,J)/RHOI
              F(I)=F1(I)*1.0E09
              K(I,1)=2.0*PI*F(I)/C
              IF(MV(I,J).NE.0.0)GO TO 450
              EDSRL=(1.0+0.508*RHOS(I,J))**3
              BC=EDSRL*EDSRL
              CC=2.0*EDSRL
              DC=3.15+CC
              EC=3.15+(2.0*BC)
              EDSCPX=3.0*VI*EPICPX(I)*BC*(CC+1.)/(DC*EC)
              EP(I,J)=CMPLX(EDSRL,-EDSCPX)
              GO TO 400
450           AI1=0.78+0.03*F1(I)-0.58*1.0E-03*(F1(I)**2)
              AI2=0.97-0.39*F1(I)*1.0E-02+0.39*1.0E-03*(F1(I)**2)
              BI1=0.31-0.05*F1(I)+0.87*1.0E-03*(F1(I)**2)
              AI3=1.0+(1.83*RHOS(I,J))+(0.02*AI1*(MV(I,J)**1.015))+BI1
              BI2=0.073*AI1
              XI1=0.073*AI2
              XI=1.31
              FOI=9.07
              AZI=F1(I)/FOI
              EDSRL=AI3+((BI2*(MV(I,J)**XI))/(1.0+AZI*AZI))
              EDSCPX=(XI1*AZI*MV(I,J)**XI)/(1.0+AZI*AZI)
              EP(I,J)=CMPLX(EDSRL,-EDSCPX)
C             WRITE(24,*)EP(I,J)
400           CONTINUE
              DO 396 J=2,6
              K(I,J)=K(I,1)*CABS(CSQRT(EP(I,J)))
396           CONTINUE
              DO 390 J=2,5
              IF(MV(I,J).EQ.0.0)GO TO 395
              T1=T-273.0
              EWINF=4.9
              EWO=88.045-0.4147*T1+6.295E-04*T1*T1+1.075E-05*T1**3
              XW=2.0*PI
              AW=1.1109E-10-3.824E-12*T1
              BW=6.938E-14*T1*T1-5.096E-16*T1**3
              TOW=(AW+BW)/XW
              CW=(XW*F(I)*TOW)**2
              DW=1.0+CW
              EPWRL=EWINF+((EWO-EWINF)/DW)
              EPWCPX=(XW*F(I)*TOW*(EWO-EWINF))/DW
```

```
          EPW(I,J)=CMPLX(EPWRL,-EPWCPX)
          MV1(I,J)=MV(I,J)/100.0
          AB=(1.0-3.0*MV1(I,J))*(EPW(I,J)-1.0)-1.0
          EPB(I,J)=(-AB+CSQRT(AB*AB+8.0*EPW(I,J)))/4.0
          GO TO 390
395       EPB(I,J)=CMPLX(1.0,-0.0)
390       CONTINUE
          DO 300 J=2,5
          VI=RHOS(I,J)/RHOI
          R(I,J)=R1(I,J)*1.0E-03
          LMDA0=C/F(I)
          EPSR(I,J)=EP(I,J)/EPB(I,J)
          AK=(EPSR(I,J)-1.0)/(EPSR(I,J)+2.0)
          ZZ=AIMAG(-AK)
          KAI(I,J)=(6.0*PI*VI*ZZ*CABS(EPB(I,J)))/LMDA0
          IF(MV(I,J).EQ.0.0)GO TO 380
          KAB(I,J)=2.0*K(I,J)*(1.0-VI)*ABS(AIMAG(CSQRT(EPB(I,J))))
          GO TO 370
380       KAB(I,J)=0.0
370       KA(I,J)=KAI(I,J)+KAB(I,J)
          CA=32.0*PI**4*R(I,J)**3*VI*(CABS(AK))**2*CABS(EPB(I,J))**4
          DA=LMDA0**4
          KS(I,J)=CA/DA
          KE(I,J)=KS(I,J)+KA(I,J)
          ALB(I,J)=KS(I,J)/KE(I,J)
300       CONTINUE
          THET0=0.0
250       THET(I,1)=THET0*PI/180.0
          DO 200 J=2,6,1
          X(I,J)=CABS(CSQRT(EP(I,(J-1))/EP(I,J)))
          Y(I,J)=X(I,J)*SIN(THET(I,(J-1)))
          THET(I,J)=ASIN(Y(I,J))
200       CONTINUE
          DO 150 J=2,5
          L(I,J)=EXP(KE(I,J)*H(I,J)/COS(THET(I,J)))
C         WRITE(24,*)L(I,J)
150       CONTINUE
          ZV(I,1)=Z(I,1)/COS(THET(I,1))
          ZH(I,1)=Z(I,1)*COS(THET(I,1))
          DO 75 J=2,6
          ZV(I,J)=(ZV(I,(J-1))*COS(THET(I,J))/CSQRT(EP(I,J)))
          ZH(I,J)=(ZH(I,(J-1))/(COS(THET(I,J))*CSQRT(EP(I,J))))
C         WRITE(24,*)ZV(I,J),ZH(I,J)
75        CONTINUE
          DO 50 J=1,5
          REF1V(I,J)=CABS((ZV(I,J)-ZV(I,(J+1)))/(ZV(I,J)+ZV(I,(J+1))))**2
          REF1H(I,J)=CABS((ZH(I,(J+1))-ZH(I,J))/(ZH(I,J)+ZH(I,(J+1))))**2
50        CONTINUE
          DO 35 J=1,5
```

```
        HDASH(I,J)=4.0*K(I,J)*K(I,J)*SIG(I,J)*SIG(I,J)
        FACT(I,J)=EXP(-HDASH(I,J)*COS(THET(I,J))**2)
        REFLV(I,J)=REF1V(I,J)*FACT(I,J)
        REFLH(I,J)=REF1H(I,J)*FACT(I,J)
35      CONTINUE
        DO 40 M=1,4
        J=6-M
        AA1=1.0-REFLV(I,(J-1))
        AA2=1.0-REFLH(I,(J-1))
        BB1=1.0-(REFLV(I,J)*REFLV(I,(J-1))/(L(I,J)*L(I,J)))
        BB2=1.0-(REFLH(I,J)*REFLH(I,(J-1))/(L(I,J)*L(I,J)))
        CC1=1.0+(REFLV(I,J)/L(I,J))
        CC2=1.0+(REFLH(I,J)/L(I,J))
        DD1=1.0-(1.0/L(I,J))
        EE1=1.0-ALB(I,J)
        FF1=((1.0-REFLV(I,J))/L(I,J))
        FF2=((1.0-REFLH(I,J))/L(I,J))
        EMISV(I,J)=AA1*((CC1*DD1*EE1)+FF1)/BB1
        EMISH(I,J)=AA2*((CC2*DD1*EE1)+FF2)/BB2
        REFLV(I,(J-1))=1.0-EMISV(I,J)
        REFLH(I,(J-1))=1.0-EMISH(I,J)
40      CONTINUE
        EMIS1(I)=1.0-REFLH(I,1)
        EMIS2(I)=1.0-REFLV(I,1)
        TB1(I)=EMIS1(I)*T
        TB2(I)=EMIS2(I)*T
        WRITE(24,*)F1(I),THETO,TB1(I),TB2(I)
        IF(THETO.GT.50.0)GO TO 500
        THETO=THETO+4.0
        GO TO 250
500     CONTINUE
        STOP
        END
```